CHMP5 controls bone turnover rates by dampening NF-κB activity in osteoclasts

Matthew B. Greenblatt,[1,2]* Kwang Hwan Park,[3,4,5]* Hwanhee Oh,[3] Jung-Min Kim,[3] Dong Yeon Shin,[3] Jae Myun Lee,[4] Jin Woo Lee,[5] Anju Singh,[6] Ki-young Lee,[7] Dorothy Hu,[8] Changchun Xiao,[9] Julia F. Charles,[10] Josef M. Penninger,[11] Sutada Lotinun,[12,13] Roland Baron,[12] Sankar Ghosh,[14] and Jae-Hyuck Shim[3]

[1]Department of Pathology, Brigham and Women's Hospital, Boston, MA 02115
[2]Department of Medicine and [3]Department of Pathology and Laboratory Medicine, Weill Cornell Medical College, New York, NY 10065
[4]Department of Microbiology, Brain Korea 21 PLUS Project for Medical Sciences and [5]Department of Orthopaedic Surgery, Yonsei University College of Medicine, Seoul 120-752, Republic of Korea
[6]National Center for Advancing Translational Sciences/National Institutes of Health, Rockville, MD 20850
[7]Department of Molecular Cell Biology and Samsung Biomedical Research Institute, Sungkyunkwan University School of Medicine, Suwon 440-746, Republic of Korea
[8]Endocrine Unit, Massachusetts General Hospital, Boston, MA 02114
[9]Department of Immunology and Microbial Science, The Scripps Research Institute, La Jolla, CA 92037
[10]Department of Medicine, Division of Rheumatology, Allergy, and Immunology, Brigham and Women's Hospital and Harvard Medical School, Boston, MA 02115
[11]Institute of Molecular Biotechnology of the Austrian Academy of Sciences, 1030 Vienna, Austria
[12]Department of Oral Medicine, Infection and Immunity, Harvard School of Dental Medicine, Boston, MA 02115
[13]Department of Physiology and STAR on Craniofacial and Skeletal Disorders, Faculty of Dentistry, Chulalongkorn University, Bangkok 10330, Thailand
[14]Department of Microbiology and Immunology, Columbia University, College of Physicians and Surgeons, New York, NY 10032

Physiological bone remodeling requires that bone formation by osteoblasts be tightly coupled to bone resorption by osteoclasts. However, relatively little is understood about how this coupling is regulated. Here, we demonstrate that modulation of NF-κB signaling in osteoclasts via a novel activity of charged multivesicular body protein 5 (CHMP5) is a key determinant of systemic rates of bone turnover. A conditional deletion of CHMP5 in osteoclasts leads to increased bone resorption by osteoclasts coupled with exuberant bone formation by osteoblasts, resembling an early onset, polyostotic form of human Paget's disease of bone (PDB). These phenotypes are reversed by haploinsufficiency for *Rank*, as well as by antiresorptive treatments, including alendronate, zolendronate, and OPG-Fc. Accordingly, CHMP5-deficient osteoclasts display increased RANKL-induced NF-κB activation and osteoclast differentiation. Biochemical analysis demonstrated that CHMP5 cooperates with the PDB genetic risk factor valosin-containing protein (VCP/p97) to stabilize the inhibitor of NF-κBα (IκBα), down-regulating ubiquitination of IκBα via the deubiquitinating enzyme USP15. Thus, CHMP5 tunes NF-κB signaling downstream of RANK in osteoclasts to dampen osteoclast differentiation, osteoblast coupling and bone turnover rates, and disruption of CHMP5 activity results in a PDB-like skeletal disorder.

Tight coupling of the activity of osteoblasts to build bone and osteoclasts to resorb bone is necessary to maintain the local biomechanical properties of bone. Moreover, this coupling activity limits the effectiveness of current therapies to treat osteoporosis, as antiresorptives targeting osteoclasts also induce a decrease in osteoblast

activity, and the ability of the PTH agonist teraparatide to promote bone formation is partially counterbalanced by increased osteoclast resorptive activity (Sims and Gooi, 2008). Thus, understanding the basis of osteoclast/osteoblast

*M.B. Greenblatt and K.H. Park contributed equally to this paper.

The Journal of Experimental Medicine

coupling is central to designing improved approaches to treat diseases of low bone mass such as osteoporosis.

Paget's disease of bone (PDB) affects 1–5% of adults over the age of 55 and is characterized by a wave of increased lytic osteoclast activity coupled with exuberant osteoblast activity, ultimately resulting in bone thickening, sclerosis, and expansion (van Staa et al., 2002; Daroszewska and Ralston, 2006; Ralston et al., 2008). These increases in osteoblast function and bone formation are believed to be driven by alterations in osteoclasts by as yet unknown coupling mechanisms (Roodman and Windle, 2005; Galson and Roodman, 2014). Notably, rare forms of PDB-like syndromes such as familial expansile osteolysis, early onset familial PBD, expansile skeletal hyperphosphatasia, juvenile PDB (JPD; familial idiopathic hyperphosphatasia), and inclusion body myopathy associated with Paget's disease of bone and frontotemporal dementia (IBMPFD) concurrently affect many bones (Daroszewska and Ralston, 2006). Risk factors influencing development of classical and rare forms of PDB include genetic variants in *CSF1*, *TNFRSF11A*, *TNFRSF11B*, *SQSTM1/p62*, *VCP/p97*, and *OPTN*, which are closely linked to the NF-κB pathway downstream of receptor activator of NF-κB (RANK), a cytokine receptor that has an essential function to drive osteoclast differentiation, and the proteasomal degradation pathway (Albagha et al., 2010, 2011). Additionally, environmental stressors such as chronic measles virus (MV) infection have been implicated in PDB development (Kurihara et al., 2011). However, despite these advances, the molecular pathobiology of both PDB development and the exaggerated coupling between osteoclast and osteoblast activities is unclear.

Previously, in an attempt to identify novel regulators of the NF-κB pathway, we identified charged multivesicular body protein 5 (CHMP5) as copurifying with the cytosolic NF-κB–IκBα complex from rabbit lung tissue extracts (Shim et al., 2006). CHMP5 is a mammalian orthologue of the yeast VPS60/MOS10 and is essential for late endosomal trafficking and multivesicular body formation as a component of the endosomal sorting complex required for transport (ESCRT) machinery (Babst et al., 2002; Köhler, 2003; Shim et al., 2006). The ESCRT machinery in turn has been demonstrated to be involved in an increasing number of diverse cellular procedures beyond traditional endocytic trafficking such as autophagy, cytokinesis, cell polarity, migration, and viral budding (Raiborg and Stenmark, 2009; Rusten et al., 2012). To study the contribution of CHMP5 to NF-κB signaling in vivo, *Chmp5*$^{-/-}$ mice were generated; however, these mice displayed embryonic lethality associated with defective lysosomal biogenesis (Shim et al., 2006). This finding largely precluded the study of the physiological contribution of CHMP5 to NF-κB signaling in vivo. Given the importance of NF-κB signaling in osteoclast biology (Jimi et al., 2004; Novack, 2011), we investigated whether CHMP5 regulates NF-κB signaling in this context using a conditional floxed allele of *Chmp5*.

Here, we demonstrate that CHMP5 dampens RANK-mediated activation of NF-κB in osteoclasts, in turn increasing the threshold of stimulation required for osteoclast differentiation and osteoclast-mediated bone resorption, thereby controlling systemic levels of bone turnover rates.

RESULTS
Expression of CHMP5 in osteoclasts
To first explore the relevance of CHMP5 to skeletal biology, we examined CHMP5 expression in long bones. Intriguingly, CHMP5 is highly expressed in mature osteoclasts in trabecular and cortical bones, whereas its expression was near the limit of detection in osteoblasts and chondrocytes in the groove of Ranvier and the growth plate (Fig. 1 A and not depicted). Accordingly, protein levels of CHMP5 were significantly increased in osteoclasts in response to RANKL (Fig. 1 B) and CHMP5 deficiency does not affect alkaline phosphatase activity (ALP) or the mineralization capacity of human BM stromal cell (BMSC)–derived osteoblasts (unpublished data). Thus, these findings imply that, among bone lineage cells, CHMP5 only functions in osteoclasts by virtue of its selective expression.

Osteoclast–specific deletion of *Chmp5* produces a high turnover, PDB–like bone phenotype
As germline deletion of *Chmp5* results in early embryonic lethality in mice (Shim et al., 2006), we generated a *Chmp5* floxed allele and bred these mice with Cathepsin K (*Ctsk*)-Cre mice (Chiu et al., 2004) to generate mice with a deletion of *Chmp5* specifically in osteoclasts (referred to herein as *Chmp5*^{Ctsk}, CKO). *Chmp5*^{Ctsk} mice were born in a Mendelian ratio, but are markedly smaller than littermate controls, though their growth rate and complete blood cell counts are comparable to those of their littermates (unpublished data). Unexpectedly, *Chmp5*^{Ctsk} mice develop early onset, severe, and progressive skeletal deformities with a Pagetoid appearance throughout both the axial and appendicular skeleton, leading to a gradual expansion of affected bones (Fig. 1, C-J). Additionally, trabecular and cortical bone mass in long bones and trabecular bone mass in vertebrae were both markedly reduced in *Chmp5*^{Ctsk} mice due to an increase in osteoclast numbers (Fig. 1, E and G). Histological analysis revealed numerous Pagetoid lesions with disorganized architecture and hyperdynamic bone as indicated by an increase in bone resorption surface area and numbers of osteoclasts specifically in these Pagetoid lesions (Fig. 1, H–J). Thus, these results demonstrate that deletion of CHMP5 in osteoclasts increases osteoclast differentiation and bone resorption activity in mice, resulting in PDB–like skeletal deformities.

Deletion of CHMP5 augments RANKL sensitivity to osteoclast differentiation
To examine the role of CHMP5 in osteoclast development, BM monocytes (BMMs) isolated from *Chmp5*$^{fl/fl}$ and *Chmp5*^{Ctsk} mice were treated with M-CSF and RANKL in vitro. During osteoclast differentiation CHMP5 expression was markedly increased in *Chmp5*$^{fl/fl}$ osteoclasts, whereas *Chmp5*^{Ctsk} osteoclasts fail to induce CHMP5 expression (Fig. 2 A). Osteoclast differentiation and sensitivity to RANKL were
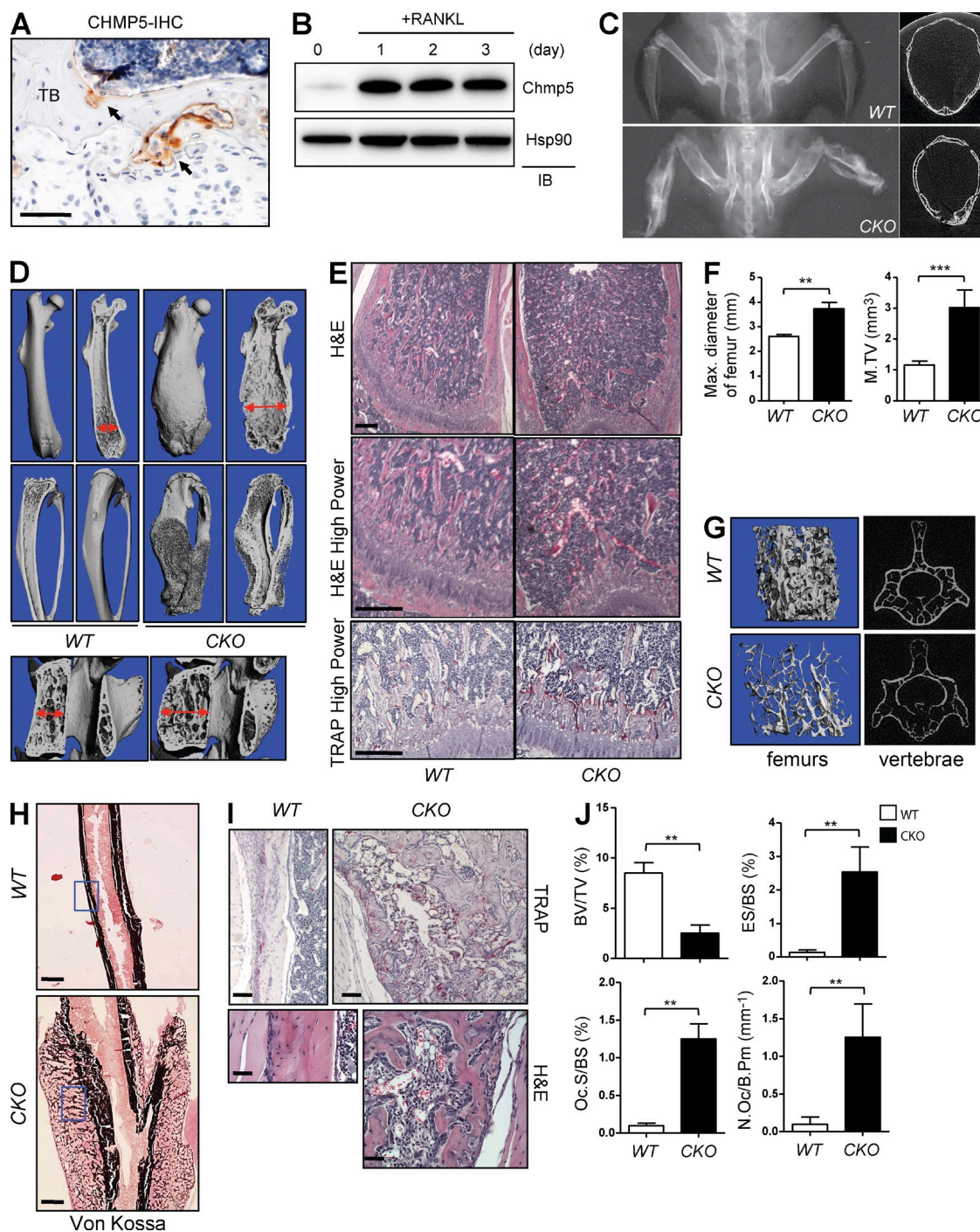
Figure 1. ***Chmp5* deletion in osteoclasts results in enhanced osteoclast differentiation and activity.** (A) Expression of CHMP5 in long bones. Immunohistochemistry for CHMP5 in the femurs of 4-wk-old male WT mice. TB, trabecular bone. Arrows indicate osteoclasts. (B) Analysis of CHMP5 expression during in vitro osteoclast differentiation of primary BMMs by immunoblotting. (C) Radiography of the hindlimbs (left) and skulls (right) of 6-wk-old male *Chmp5*^{fl/fl} and *Chmp5*^{Ctsk} mice. The images represent three mice per group. (D, F, and G) µCT analysis of the femurs, the tibias, and the vertebrae of 12-wk-old male *Chmp5*^{fl/fl} and *Chmp5*^{Ctsk} mice. Shown are representative sagittal sections of femurs (D, top), tibias (D, middle), L4 vertebrae (D, bottom) with quantification of maximal diameter of distal femur and total volume of middle femur (M.TV; F), 3D reconstructions of femurs (G, left), and cross section of L4 vertebrae (G, right). (E) Hematoxylin and eosin staining (top, low power; middle, high power) and TRAP staining (bottom, high power) of 12-wk-old male *Chmp5*^{fl/fl} and *Chmp5*^{Ctsk} femurs. (H and I) Von Kossa staining (H), TRAP staining (I, top), and hematoxylin and eosin staining (I, bottom) of 12-wk-old male *Chmp5*^{fl/fl} and *Chmp5*^{Ctsk} tibias (H) and Pagetoid lesions (I). (J) Histomorphometric analysis of 12-wk-old male *Chmp5*^{fl/fl} tibias and *Chmp5*^{Ctsk} Pagetoid lesions. $n > 5$ mice per group in D, F, G, and J. All error bars indicate SEM by the Mann-Whitney test. **, $P < 0.01$; ***, $P < 0.001$. Bars: (A) 25 µm; (E) 100 µm; (H) 300 µm; (I) 50 µm.

dramatically increased in *Chmp5^Ctsk* BMMs, as indicated by an increase in tartrate-resistant acid phosphatase (TRAP) staining and activity (Fig. 2, B–D) and osteoclast marker gene expression (Fig. 3, A and B). Likewise, *Chmp5^Ctsk* osteoclasts displaced markedly increased bone resorptive activity with a 2–3 fold increase in the number and area of resorption pits and in the liberation of type I collagen C-terminal telopeptide (CTX; Fig. 2 E). This increase in resorptive activity likely reflected both increased differentiation and proliferation, as carboxyfluorescein succinimidyl ester (CFSE) labeling demonstrated increased proliferation of *Chmp5^Ctsk* BMMs under osteoclast differentiation conditions (unpublished data). Similar to observations made in human PDB patients (Rebel et al., 1974), *Chmp5^Ctsk* osteoclasts were larger and contained more nuclei than *Chmp5^fl/fl* osteoclasts (Fig. 2 F).

Osteoclast differentiation is accompanied by cytoskeletal reorganization necessary to orient the resorptive machinery toward the bone surface and to seal around the resorption pit (Teitelbaum and Ross, 2003) where the Src protooncogenes serve as key regulators of this process (Soriano et al., 1991; Zou et al., 2007; Izawa et al., 2012). Intriguingly, *Chmp5^Ctsk* osteoclasts show elevated levels and activation of Src and increases in the activation of the downstream effectors Syk and active GTP-bound Rac1 (Fig. 2, G–I). In keeping with these observations, actin ring formation was enhanced in *Chmp5^Ctsk* osteoclasts (Fig. 2 J). Thus, CHMP5 coordinately regulates several aspects of osteoclast differentiation necessary for resorptive activity.

Deletion of CHMP5 augments production of osteoblast/osteoclast coupling factors in osteoclasts

To determine how CHMP5 regulates gene expression in osteoclasts, we performed RNA sequencing analysis of *Chmp5^fl/fl* and *Chmp5^Ctsk* osteoclasts. As expected, gene-set enrichment analysis (GSEA) showed an enrichment of genes associated with osteoclast differentiation and fusion in *Chmp5^Ctsk* osteoclasts, and the increase in gene expression was confirmed by RT-PCR analysis (Fig. 3, A and B). Expression of IL-6, a signature gene of Pagetic osteoclasts (Hoyland et al., 1994; Roodman et al., 1992; Roodman and Windle, 2005) was also increased by 3–4-fold in *Chmp5^Ctsk* osteoclasts (Fig. 3 C). Intriguingly, genes associated with Ephrin B-mediated reverse signaling were enriched in *Chmp5^Ctsk* osteoclasts (Fig. 3 D; Zhao et al., 2006). Additionally, *Chmp5^Ctsk* osteoclasts show an increase in expression of several clastokines, secreted osteoclast-derived coupling factors that promote osteoblast activity, including *Efnb2* (Zhao et al., 2006), *Sphk1* (Ryu et al., 2006), *Cthrc1* (Takeshita et al., 2013), *Wnt10b* (Ota et al., 2013), and *Bmp6* (Teti, 2013; Fig. 3 E). The high expression of several clastokines in *Chmp5^Ctsk* osteoclasts prompted us to examine the ability of *Chmp5^Ctsk* osteoclasts to promote osteoblast differentiation. Co-culture with *Chmp5^Ctsk* osteoclasts increased mineralization and ALP activity to a greater extent than that seen with corresponding WT controls (Fig. 4, A and B). As the same effects were observed with conditioned medium from *Chmp5^Ctsk* osteoclasts, CHMP5–deficient osteoclasts also promote osteoblast differentiation in vitro via secreted coupling factors (Fig. 4 C).

Signaling between EphB4 on osteoblasts and its primary ligand ephrinB2 on osteoclasts stimulates osteoblast differentiation (Zhao et al., 2006). To determine the contribution of the EphrinB2–EphB4 pathway to the enhanced osteoblast coupling seen in *Chmp5^Ctsk* osteoclasts, EphB4-Fc fusion protein was added to osteoclast/osteoblast co-cultures to suppress EphrinB2–EphB4 signaling (Fig. 4, D and E). Treatment with EphB4-Fc decreased osteoblast mineralization activity, reversing the effect of *Chmp5^Ctsk* osteoclasts to promote osteoblast differentiation. Thus, the EphrinB2–EphB4 pathway is likely to be one important contributor to the enhanced osteoblast coupling activity of *Chmp5^Ctsk* osteoclasts, though other pathways are likely to contribute as well.

Next, we examined the in vivo expression levels of the coupling factors known to be important for bone remodeling by RNA sequencing of marrow-flushed tibias. As shown in Fig. 4 F, *Chmp5^Ctsk* long bones showed elevated levels of both osteogenic factors such as *Tgbf1* (Tang et al., 2009), *Igf1* (Xian et al., 2012), and *Lif* (Cornish et al., 1997) and an osteoclastogenic factor *Csf1 (Wei et al., 2006)*, whereas expression of other genes, including *Cxcl12*, *Fgf2*, *Bmp2*, and *Bmp6* in *Chmp5^Ctsk* long bones was comparable to levels in *Chmp5^fl/fl* bones. An elevated Rankl/Opg ratio was also observed in *Chmp5^Ctsk* long bones, suggesting an increase in bone remodeling activity (Fig. 4 G). As reported in BMSCs and osteoblasts isolated from PDB patients (Naot et al., 2007), *Chmp5^Ctsk* long bones show distinct patterns of expression of two WNT signaling antagonists, an increased expression of Dickkopf1 (*Dkk1*) and a decreased expression of Sclerostin (*Sost*; Fig. 4 H). Collectively, *Chmp5* deletion in osteoclasts enhances transcriptional programs corresponding to osteoclast differentiation/activity and also augments production of osteoclast–osteoblast coupling factors.

Osteoblast activity is highly increased in *Chmp5^Ctsk* mice

To examine whether the elevated levels of the coupling factors observed in *Chmp5^Ctsk* osteoclasts correspond to increased osteoblast activity in vivo, dynamic histomorphometry analysis was conducted. As seen in Fig. 5 (A–B), bone formation rate, mineral apposition rate, and numbers of osteoblasts are markedly increased in periosteal Pagetic lesions. Likewise, in situ hybridization demonstrated increased numbers of mature osteoblasts expressing type 1 collagen α1 (Col1) and osteocalcin (Ocn) in these bone lesions (Fig. 5 C). Consistent with a previous study showing that mature osteoblasts express high levels of vascular endothelial growth factors (VEGFs) and with clinical observations that Pagetoid lesions are hypervascular to the point of occasionally causing high-output heart failure in severe polyostotic cases (Chakravorty, 1978; Zajac and Phillips, 1985; Deckers et al., 2000), these bone lesions are hypervascular and display elevated levels of VEGF expression (Fig. 5, D–F). Additionally, the serum levels of the bone turnover markers ALP, CTX, and N-terminal propeptide of type 1 procollagen (P1NP) were all significantly increased in
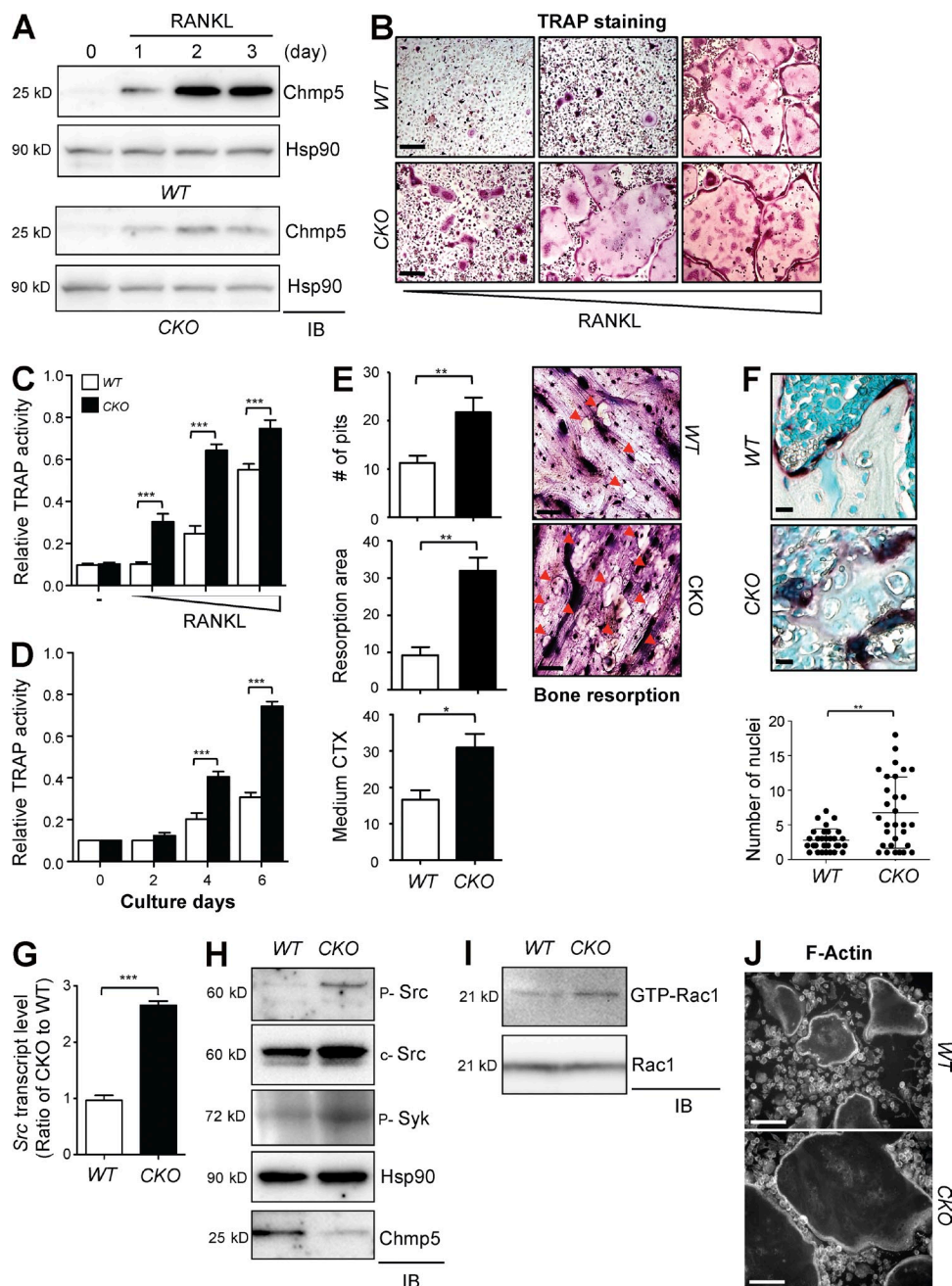
Figure 2.   *Chmp5* deletion leads to an increase in osteoclast differentiation and RANKL responsiveness. (A–C) *Chmp5^{fl/fl}* and *Chmp5^{Ctsk}* BMMs were cultured with 40 ng/ml of M-CSF and 20 ng/ml of RANKL for the indicated time periods, and cell lysates were immunoblotted with the indicated antibodies (A). Alternatively, BMMs were cultured with different concentrations of RANKL and multinucleated cells were stained with TRAP (B), and then TRAP activity was measured by colorimetric analysis (C) after 6 d of culture. ***, P < 0.005 by a Bonferroni-corrected two-tailed Student's *t* test. (D) *Chmp5^{fl/fl}* and *Chmp5^{Ctsk}* BMMs were cultured with 40 ng/ml of M-CSF and 10 ng/ml of RANKL for the indicated time periods and TRAP activity was measured by colorimetric analysis. ***, P < 0.005 by a Bonferroni-corrected two-tailed Student's *t* test. (E) Bone resorptive activity of *Chmp5^{fl/fl}* and *Chmp5^{Ctsk}* osteo-clasts. Shown are representative images of in vitro bone resorption assays (right) with quantification of pit number, resorption area, and medium CTX (left, nM). *, P < 0.05; **, P < 0.01 by a two-tailed Student's *t* test. Red arrows indicate bone resorption pits. *n* = 5 fields/slide. (F) Photomicrographs of TRAP-positive osteoclasts in *Chmp5^{fl/fl}* trabecular bone and Pagetoid lesions in *Chmp5^{Ctsk}* mice (*CKO*; left). Additionally, the number of nuclei in TRAP-positive osteoclasts was counted (*n* = 30 cells/slide). **, P < 0.01 by a Bonferroni-corrected two-tailed Student's *t* test. (G) Elevated levels of *Src* tran-scripts in *Chmp5^{Ctsk}* osteoclasts. RT-PCR analysis was performed with total RNAs isolated from cultured *Chmp5^{fl/fl}* and *Chmp5^{Ctsk}* osteoclasts after 4 d of culture. ***, P < 0.001 by a Bonferroni-corrected two-tailed Student's *t* test. (H and I) After 4 d of culture, *Chmp5^{fl/fl}* and *Chmp5^{Ctsk}* osteoclasts were lysed and immunoblotted with the indicated antibodies (H). Alternatively, GTP-bound Rac1 and total Rac 1 were determined by immunoblotting with anti-Rac 1 antibody (I). (J) Enlarged actin rings in *Chmp5^{Ctsk}* osteoclasts. *Chmp5^{fl/fl}* and *Chmp5^{Ctsk}* osteoclasts were immunostained with FITC-phalloidin. *n* = 3 independent experiments in A–D and F–J. All error bars indicate SEM. Bars: (B) 60 µm; (E) 100 µm; (F) 25 µm; (J) 100 µm.
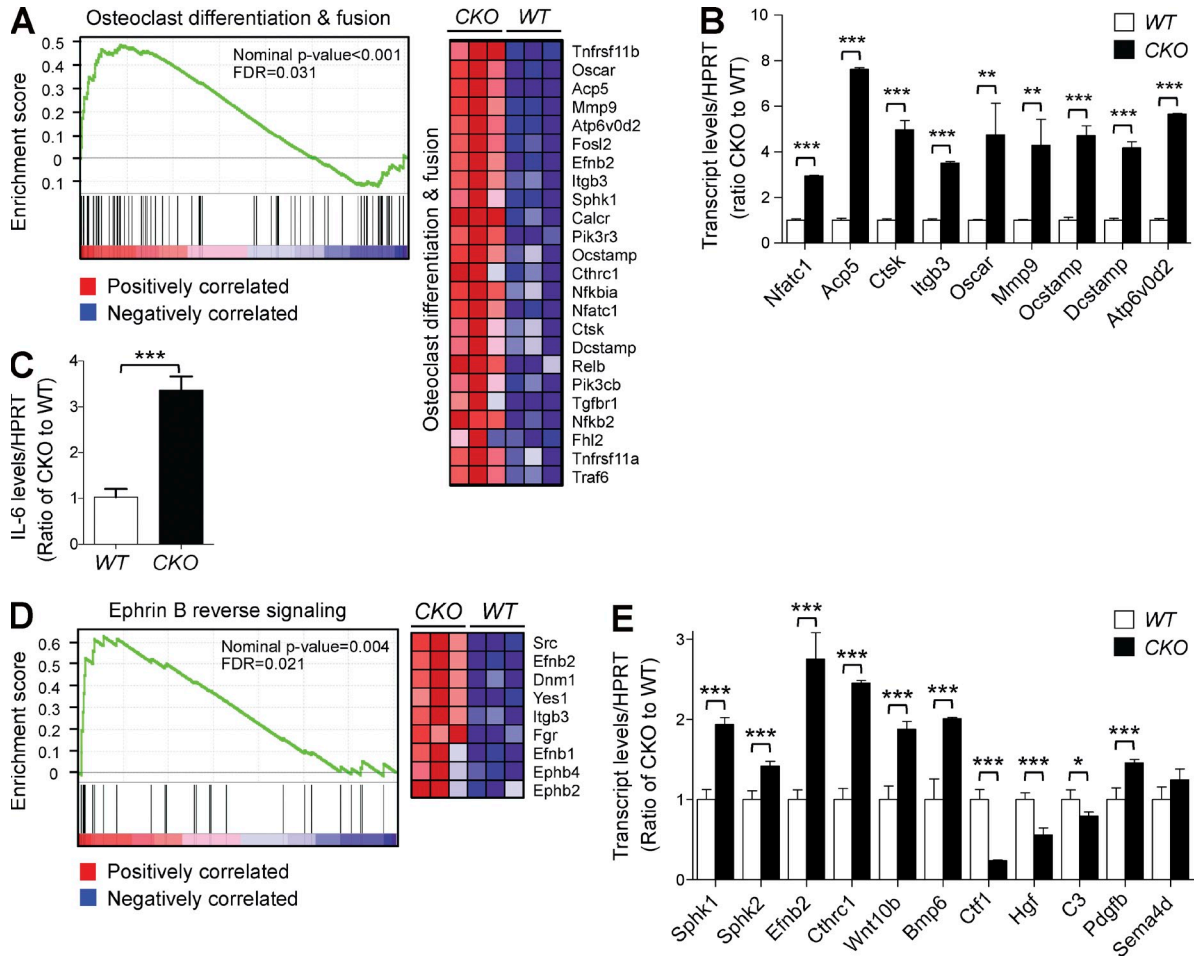
Figure 3. Elevated levels of genes involved in osteoclast differentiation and clastokines in *Chmp5^{Ctsk}* osteoclasts. (A and D) Enrichment plots (left) and signature genes (right) in *Chmp5^{fl/fl}* and *Chmp5^{Ctsk}* osteoclast culture (*n* = 3 mice/group). GSEA analysis displays enrichment of genes involved with osteoclast differentiation and fusion (A) and Ephrin B reverse signaling (D). (B) Expression of the genes involved with osteoclast differentiation and fusion is highly increased in *Chmp5^{Ctsk}* osteoclast culture. RT-PCR analysis was performed with total RNAs isolated from cultured *Chmp5^{fl/fl}* and *Chmp5^{Ctsk}* osteoclasts (*n* = 3 mice/group). (C and E) Expression of IL-6 (C) and known clastokines (E) in cultured *Chmp5^{fl/fl}* and *Chmp5^{Ctsk}* osteoclasts was measured by RT-PCR analysis (*n* = 3 mice/group). Data in B, C, and E represent *n* = 3 independent experiments. All error bars indicate SEM. *, $P < 0.05$; **, $P < 0.01$; ***, $P < 0.001$ by Bonferroni-corrected two-tailed Student's *t* tests.

Chmp5^{Ctsk} mice, consistent with a high bone turnover state (Fig. 5 G). Given that CHMP5 expression and osteoblast differentiation and activity were all normal in the cultured osteoblasts from *Chmp5^{Ctsk}* bone marrow stromal cells (BMSCs; unpublished data), this strongly suggests that the high bone turnover state is intrinsic to the function of CHMP5 in osteoclasts. Collectively, *Chmp5^{Ctsk}* mice demonstrate a high bone turnover state complete with early onset and polyostotic de novo formation of expansile Pagetoid lesions on periosteal surfaces. In this respect, the phenotype of *Chmp5^{Ctsk}* mice best resembles the severe polyostotic forms of Paget's seen in human JPD or other heritable PDB-like disorders such as familial expansile osteolysis (Bakwin and Eiger, 1956) as opposed to typical sporadic PDB that typically manifests as focal lesions in patients over age 50 (Daroszewska and Ralston, 2006; Galson and Roodman, 2014).

Antiresorptive treatments reverse the PDB–like bone phenotype of *Chmp5^{Ctsk}* mice

To examine if the increased sensitivity of *Chmp5^{Ctsk}* osteoclasts to RANKL observed in vitro was responsible for the PDB-like bone phenotypes observed in vivo, the genetic interaction between CHMP5 and the RANKL receptor RANK was examined by comparing *WT*, *Rank^{+/−} (Rank-Het)*, *Chmp5^{Ctsk} (CKO)*, and *Chmp5^{Ctsk};Rank^{+/−} (CKO;Rank-Het)* mice (Fig. 6). Though *Rank-Het* mice do not display detectable bone phenotypes at baseline (Dougall et al., 1999), *CKO;Rank-Het* mice displayed a substantial reversal of the PDB-like bone phenotypes in *Chmp5^{Ctsk}* mice, including low trabecular bone mass, bone expansion, and the existence of Pagetoid lesions (Fig. 6, A–E). Additionally, elevated numbers of osteoclasts and high serum levels of bone turnover markers observed in the *CKO* mice were largely normalized
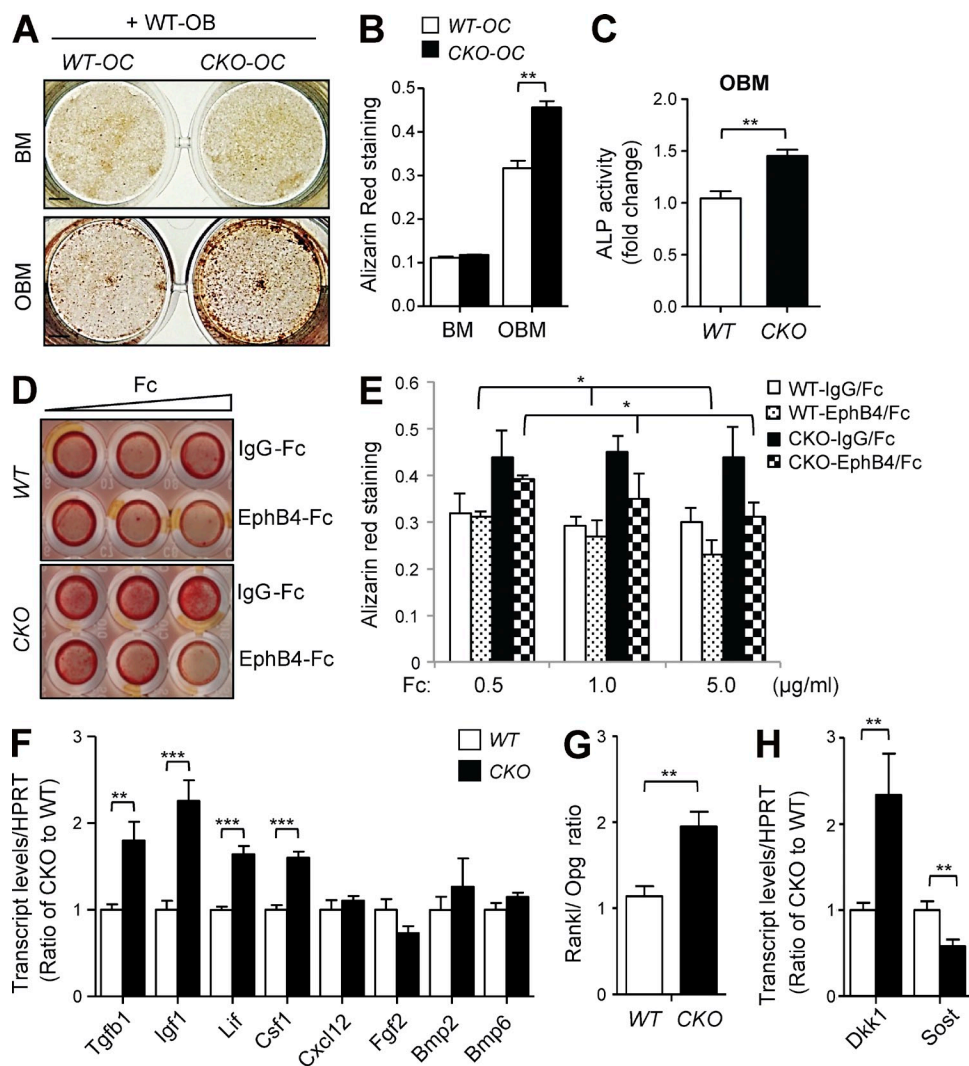
Figure 4. ***Chmp5*** *Ctsk* **osteoclasts promote osteoblastogenesis and bone remodeling.** (A and B) Primary calvarial osteoblasts were co-cultured with *Chmp5* *fl/fl* (WT-OC) and *Chmp5* *Ctsk* (CKO-OC) BMMs in basal (BM) or osteoblast differentiation medium (OBM) in the presence of M-CSF and RANKL, and then stained with alizarin red (A); alizarin red was then measured by colorimetric analysis for mineralization activity (B). **, P < 0.01 by a Bonferroni-corrected two-tailed Student's *t* test. (C) Primary calvarial osteoblasts were cultured under OBM in the presence of conditioned medium (CM) collected from *Chmp5* *fl/fl* (*WT*) and *Chmp5* *Ctsk* (*CKO*) osteoclasts, and alkaline phosphatase activity (ALP) was measured to assess osteoblast differentiation. **, P < 0.01 by a Bonferroni-corrected two-tailed Student's *t* test. (D and E) Various concentrations of mouse IgG-Fc or EphB4-Fc fusion proteins were added to the co-culture of osteoblasts and *Chmp5* *fl/fl* or *Chmp5* *Ctsk* BMMs in osteoblast differentiation medium containing M-CSF and RANKL. Mineralization activity was assessed by alizarin red staining. *, P < 0.05 by a Bonferroni-corrected two-tailed Student's *t* test. (F–H) Total RNA was isolated from 6-wk-old male *Chmp5* *fl/fl* and *Chmp5* *Ctsk* tibias (*n* = 6 mice/group) for RT-PCR analysis. Data in A–C and E–H represent *n* = 3 independent experiments. All error bars indicate SEM. **, P < 0.01; ***, P < 0.001 by a Bonferroni-corrected two-tailed Student's *t* test. Bar: (A) 5 mm.

by *Rank* haploinsufficiency (Fig. 6, D–F). Thus, a partial reduction in RANK expression levels imparted by *Rank* haploinsufficiency can reverse the PDB-like bone phenotype of *Chmp5* *Ctsk* mice, arguing that the ability of CHMP5 deletion to increase osteoclast responsiveness to RANK stimulation is central to the pathogenesis of the PDB-like skeletal disorder in *Chmp5* *Ctsk* mice.

Previous case reports have suggested that treatment of patients with JPD with antiresorptives such as bisphosphonates, recombinant OPG, or the anti-RANKL antibody Denosumab

can potentially reduce their rate of bone turnover and prevent the development of skeletal deformity (Cundy et al., 2004, 2005; Polyzos et al., 2014). Thus, assessment of the response of *Chmp5* *Ctsk* mice to antiresorptives is important to determine the relevance of the model to human PDB-spectrum disorders and also to mechanistically evaluate the contribution of RANKL signaling. *Chmp5* *fl/fl* or *Chmp5* *Ctsk* mice were treated with PBS, alendronate, zolendronate, or recombinant osteoprotegerin-Fc fusion (OPG-Fc) weekly from 2–6 wk of age (Fig. 7). The low bone mass, bone expansion, and elevated
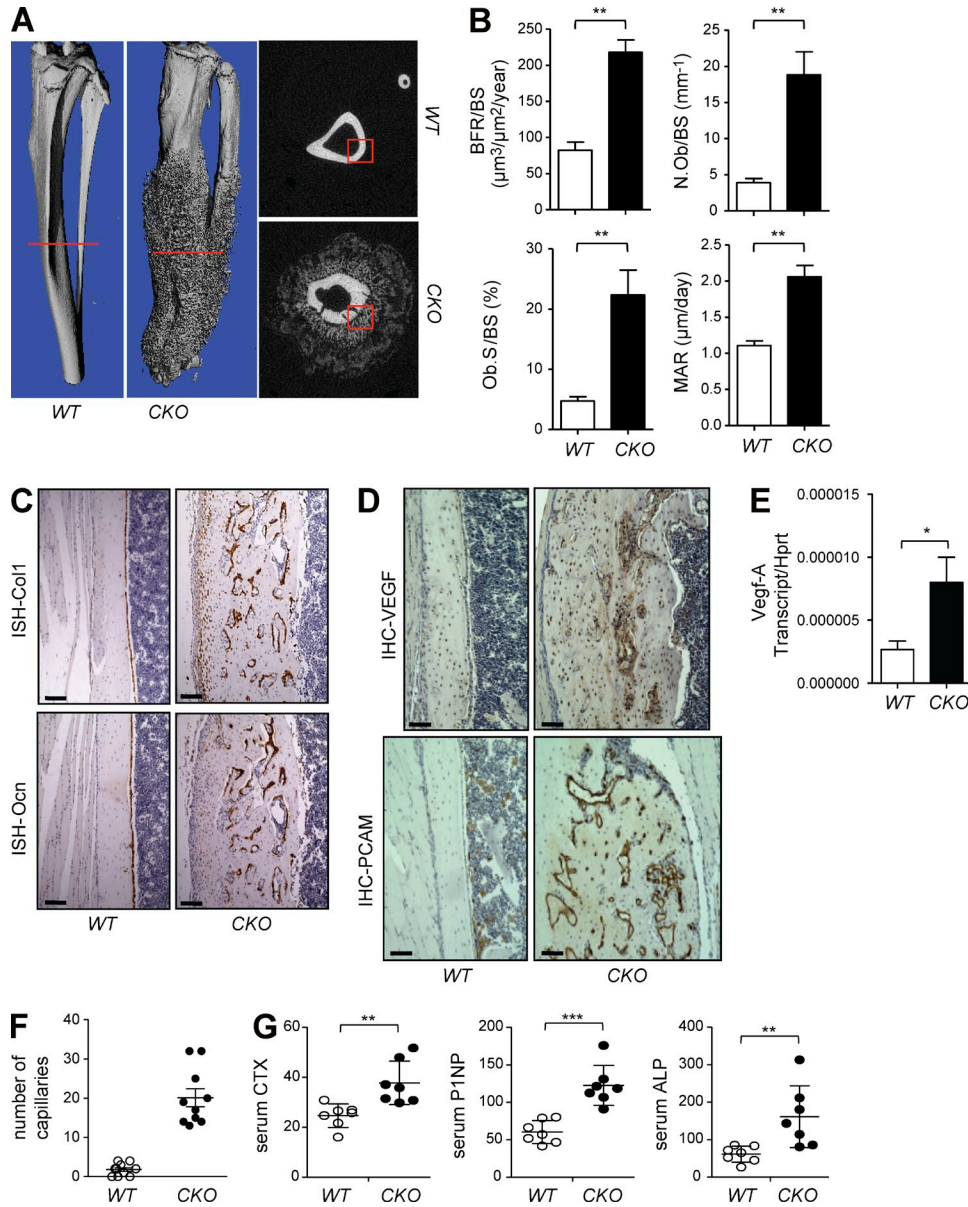
Figure 5. ***Chmp5^{Ctsk}* mice display enhanced osteoblast activity and angiogenesis in Pagetoid lesions.** (A) μCT analysis of 12-wk-old male *Chmp5^{fl/fl}* and *Chmp5^{Ctsk}* tibias. Shown are representative 3D reconstructions of tibias (left) and images showing the cross sections corresponding to the red lines (right). Red box indicates the area analyzed for histomorphometry. (B) Histomorphometric analysis of 12-wk-old male *Chmp5^{fl/fl}* tibias and *Chmp5^{Ctsk}* periosteal Pagetoid lesions. *n* > 5 mice/group. **, P < 0.01 by a Bonferroni-corrected two-tailed Student's *t* test. (C, D, and F) In situ hybridization for *Col1* and *Ocn* (C) and immunohistochemistry for VEGF and PCAM (D) of Pagetoid lesions in *Chmp5^{Ctsk}* femurs. Number of capillaries in cross section of cortical bones (*n* = 10 fields/slide from 5 randomized mice/group). (F) Cortical bones of 12-wk-old male *Chmp5^{fl/fl}* mice were used as WT control. **, P < 0.01 by a Bonferroni-corrected two-tailed Student's *t* test. (E) Total RNA was isolated from 6-wk-old male *Chmp5^{fl/fl}* and *Chmp5^{Ctsk}* tibias, and *Vegf-A* expression was measured by RT-PCR (*n* = 6 mice/group). *, P < 0.05 by a Bonferroni-corrected two-tailed Student's *t* test. (G) Serum levels of CTX, P1NP, and ALP in 12-wk-old male *Chmp5^{fl/fl}* and *Chmp5^{Ctsk}* mice (*n* = 7 mice/group). **, P < 0.01 by a Bonferroni-corrected two-tailed Student's *t* test. Bars: (C and D) 50 μm.

serum levels of bone turnover markers observed in *Chmp5^{Ctsk}* mice were reversed by treatment with antiresorptive agents. Osteoclast differentiation was completely abolished by OPG-Fc treatment, whereas treatment with bisphosphonates blocked bone resorption activity (Fig. 7, D–F). Overall, OPG-Fc elicited a more substantial reversal of the phenotype of *Chmp5^{Ctsk}*

mice than either alendronate or zolendrate. Coupled with the finding that *Rank* haploinsufficiency rescues the *Chmp5^{Ctsk}* phenotype, this result confirms that the development of the PDB–like phenotype in *Chmp5^{Ctsk}* mice is highly dependent on the relative levels of RANK signaling and osteoclast differentiation/activity in vivo.
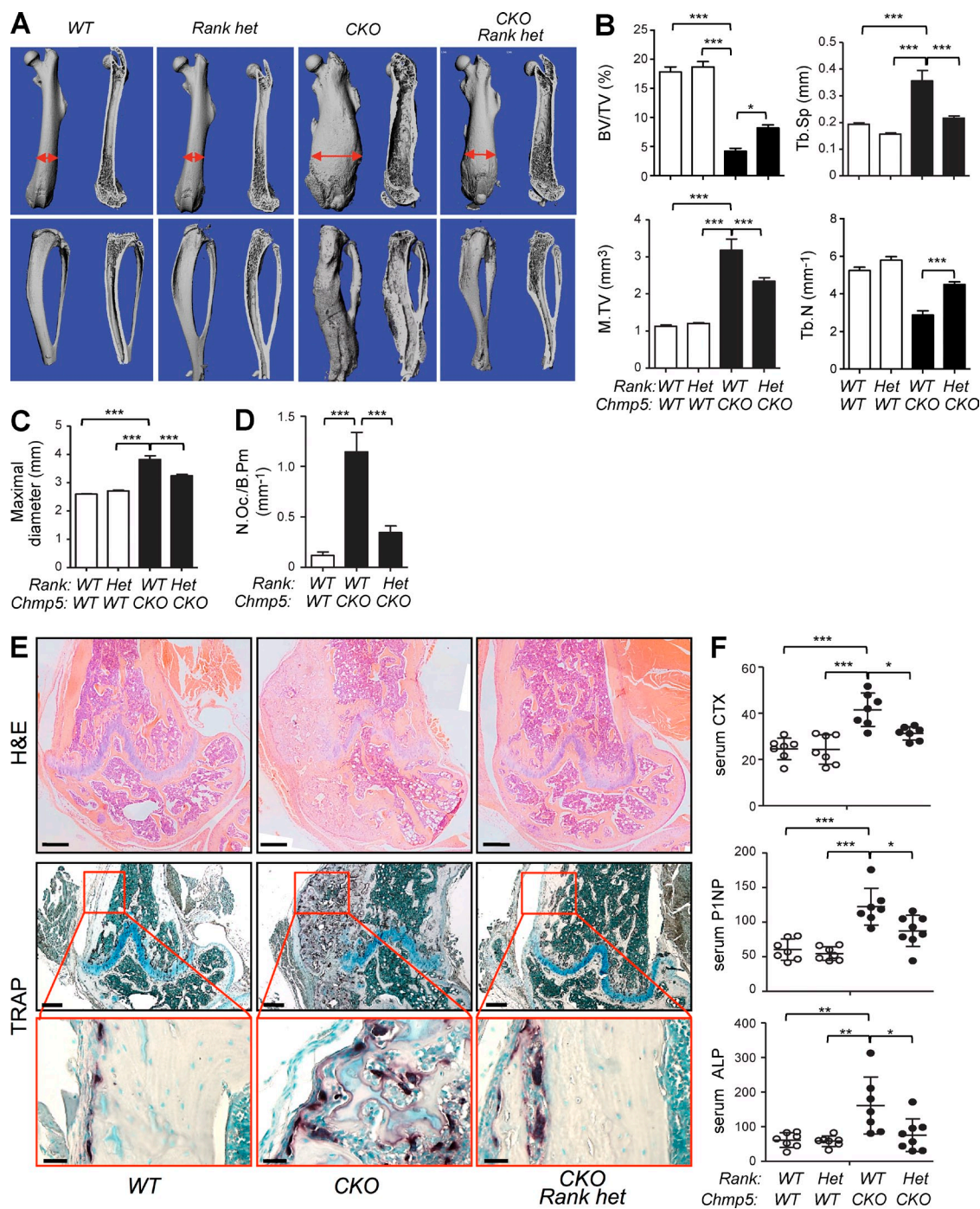
Figure 6. *Rank* haploinsufficiency reverses PDB–like bone phenotypes in *Chmp5^Ctsk* mice. (A–C) μCT analysis of the femur and tibia of 12-wk-old male *Rank^+/+;Chmp5^fl/fl (WT)*, *Rank^+/Δ;Chmp5^fl/fl (Rank het)*, *Rank^+/+;Chmp5^Ctsk (CKO)*, and *Rank^+/Δ;Chmp5^Ctsk (CKO;Rank het)* mice. Shown are representative 3D reconstructions of femurs and tibias (A) with quantification of bone volume/total volume (BV/TV), trabecular separation (Tb.Sp), trabecular number (Tb.N), midshaft volume (M. TV), and maximal femoral diameter. (B and C; n = 7 mice/group). Red arrows indicate maximal femoral diameter. *, P < 0.05; **, P < 0.01; ***, P < 0.001 by a Bonferroni-corrected two-tailed Student's *t* test. (D and E) Femurs of the indicated mice were stained for histological analysis, including hematoxylin and eosin and TRAP staining, and the images are compilation/mosaics (E). TRAP-positive osteoclasts were counted in trabecular bones of *WT* and *CKO;Rank het* mice and Pagetoid lesions in *CKO* mice (n = 7 mice/group; D). ***, P < 0.001 by a Bonferroni-corrected two-tailed Student's *t* test. (F) Serum levels of CTX, P1NP, and ALP in 12-wk-old male *WT, Rank het, CKO,* and *CKO;Rank het* mice (n = 7 mice/group). *, P < 0.05; **, P < 0.01; ***, P < 0.001 by a Bonferroni-corrected two-tailed Student's *t* test. All error bars indicate SEM. Bars: (E, top and middle) 100 μm; (E, bottom) 25 μm.
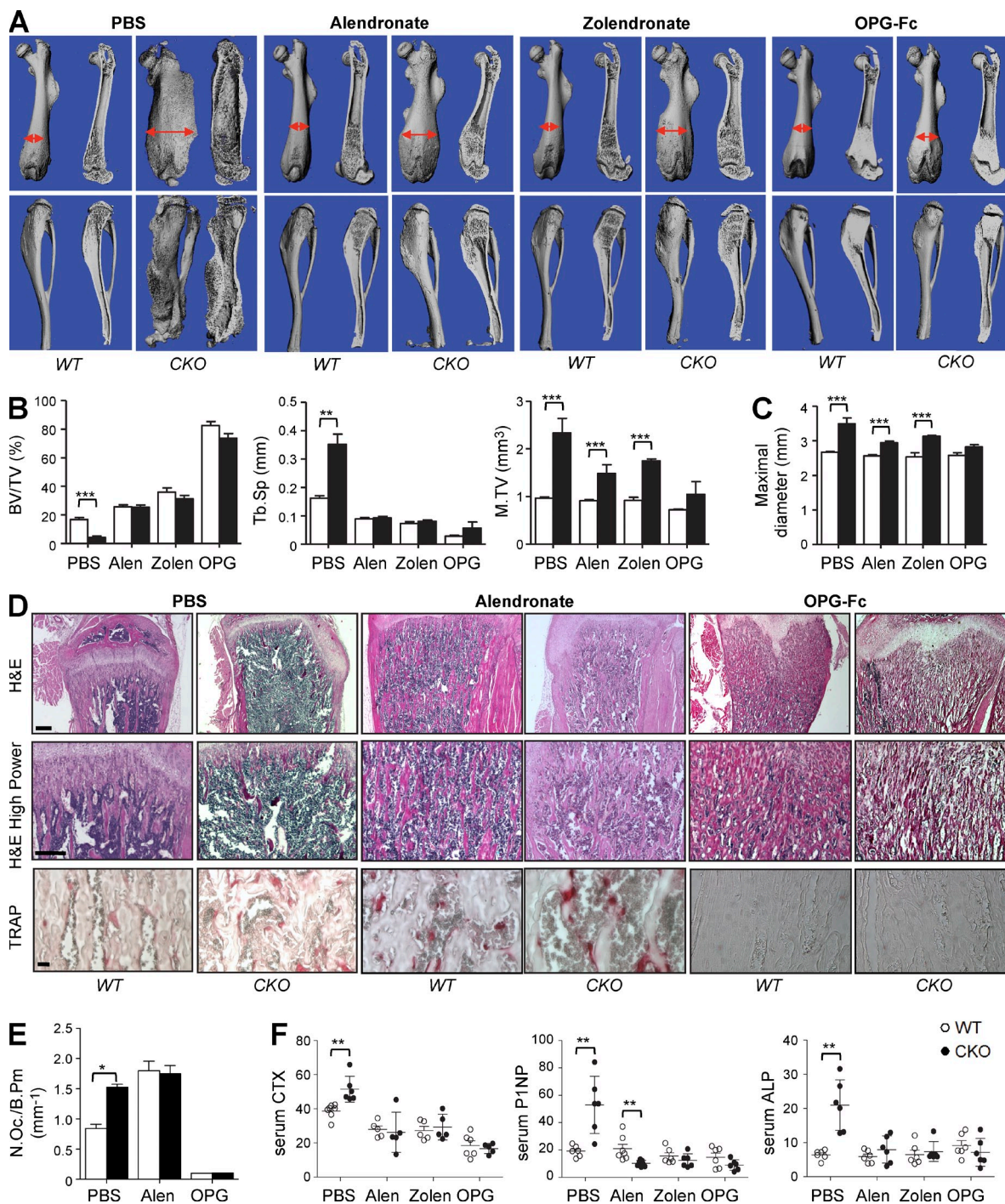
Figure 7. **Antiresorptive treatments reverse PDB–like bone phenotypes in *Chmp5^Ctsk* mice.** (A–C) μCT analysis of the femurs and tibias in 6-wk-old male *Chmp5^fl/fl* and *Chmp5^Ctsk* mice. Mice were randomized to treatment with PBS, alendronate (Alen), zolendronate (Zolen), or OPG-Fc (OPG) weekly from 2–5-wk-old via IP injection. Shown are representative 3D reconstructions of femurs and tibias (A) with quantification of bone volume/total volume (BV/TV), trabecular separation (Tb.Sp), midshaft volume (M. TV), and maximal femoral diameter (B and C; *n* = 5 mice/group). Red arrows indicate maximal diameter. **, P < 0.01; ***, P < 0.001 by a Bonferroni-corrected two-tailed Student's *t* test. (D and E) Femurs of the indicated mice were stained for histological analysis, including hematoxylin and eosin and TRAP staining. RAP-positive osteoclasts were counted in trabecular bones of *Chmp5^fl/fl* and *Chmp5^Ctsk* mice treated with PBS, alendronate, or OPG-Fc (*n* = 5 mice/group; E). *, P < 0.05 by a Bonferroni-corrected two-tailed Student's *t* test. (F) Serum levels of CTX, P1NP, and ALP in 6-wk-old male *Chmp5^fl/fl* and *Chmp5^Ctsk* mice treated with PBS, Alen, Zolen, or OPG (*n* = 5 mice/group). All error bars indicate SEM. **, P < 0.01 by a Bonferroni-corrected two-tailed Student's *t* test. Bars: (D, top and middle) 100 μm; (D, bottom) 25 μm.
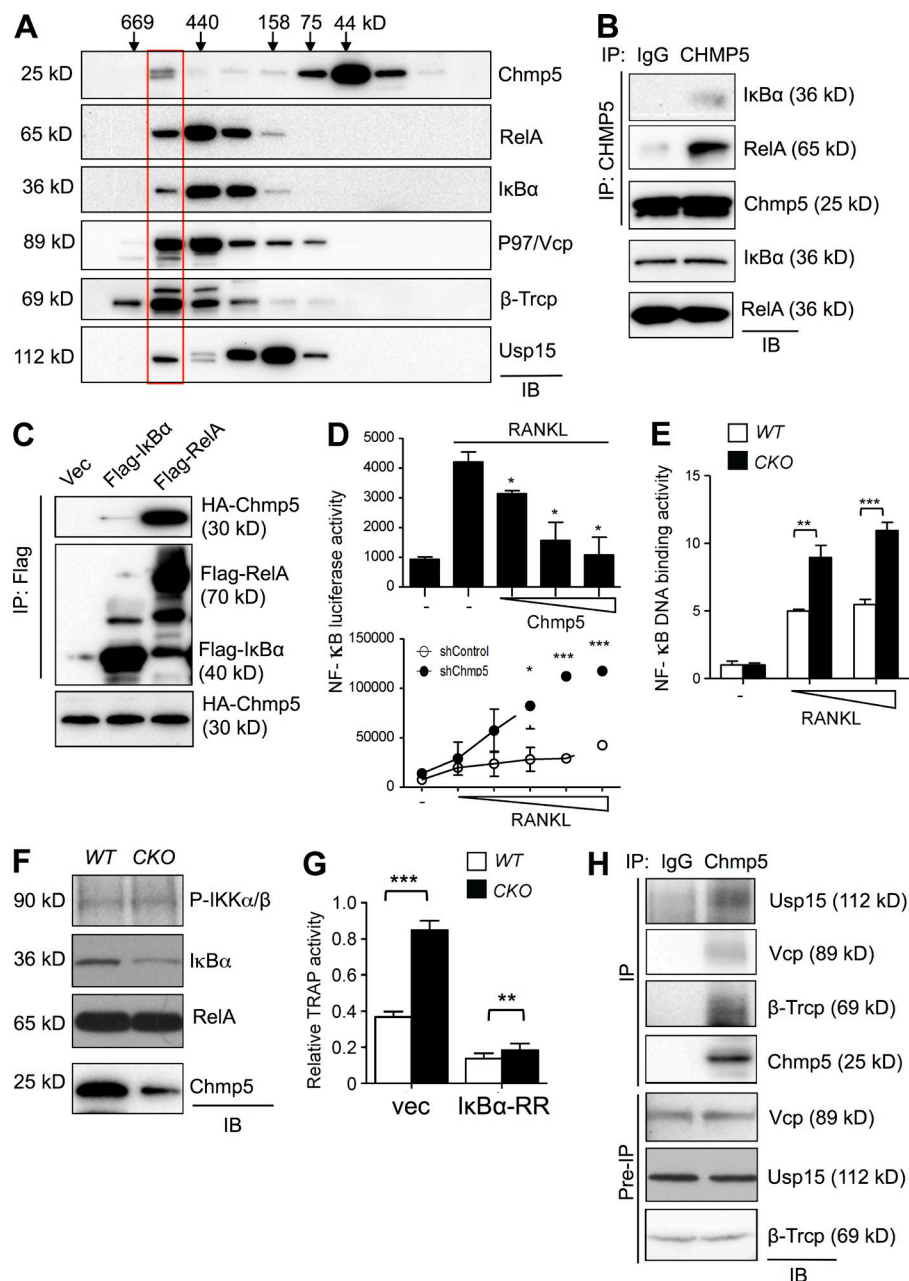
Figure 8. CHMP5 down-regulates RANK-mediated NF-κB activation in osteoclasts. (A, B, and H) Fractionation of the CHMP5 protein complex in osteoclasts. RAW264.7 cells were lysed with 1% CHAPS lysis buffer and fractionated by size exclusion chromatography. The fractions were immunoblotted with the indicated antibodies (A). The fraction in the red box was immunoprecipitated with anti-Chmp5 antibody or IgG control antibody along with protein G–conjugated dynabeads, and immunoblotted with the indicated antibodies (B and H). The images in A, B, and H represent two independent experiments. (C) HEK293 cells were transfected with HA-Chmp5 along with vector or Flag tagged-IκBα or -RelA. After 48-h transfection, the cells were lysed, immunoprecipitated with anti-Flag antibody–conjugated agarose, and immunoblotted with the indicated antibodies. (D) RAW264.7 cells were transfected with Chmp5 in a dose-dependent manner along with PBII-luc and *Renilla* and stimulated with 50 ng/ml of RANKL (top) or RAW264.7 cells expressing control, or Chmp5 shRNA were treated with different concentrations of RANKL (bottom). Relative luciferase activity was normalized to *Renilla*. *, P < 0.05; ***, P < 0.0001 by a Bonferroni-corrected two-tailed Student's *t* test. (E-G) *Chmp5^fl/fl* and *Chmp5^Ctsk* BMMs were cultured in the presence of M-CSF and RANKL, and after 3 d total cell lysates were used for an NF-κB DNA-binding assay (E) or immunoblotted with the indicated antibodies (F). Alternatively, BMMs were infected by lentiviruses expressing vector or the super repressor, HA-IκBα-RR, and osteoclast differentiation was measured by TRAP activity (G). **, P < 0.01; ***, P < 0.0001 by a Bonferroni-corrected two-tailed Student's *t* test.

CHMP5 suppresses RANK-mediated NF-κB activation in osteoclasts

We previously reported that CHMP5 functions as a negative regulator of NF-κB signaling downstream of proinflammatory cytokines, though the mechanism of this effect was unclear (Shim et al., 2006). Size-exclusion chromatography of the preosteoclast line Raw 264.7 showed that endogenous CHMP5 cofractionated with a subset of NF-κB RelA and IκBα in an ∼550-kD complex (Fig. 8 A). Immunoprecipitation analysis confirmed that both endogenous and overexpressed CHMP5 interacts with RelA and IκBα in an osteoclast line and HEK293 cells, respectively (Fig. 8, B and C). However, the interactions with NF-κB p50, NF-κB p100, and

IκBβ were not observed, indicating selective interactions between CHMP5 and NF-κB and IκB isoforms (unpublished data). In this context, luciferase assay with a NF-κB responsive reporter showed that RANKL-induced NF-κB activation was significantly inhibited by CHMP5 overexpression, whereas CHMP5 deficiency enhanced RANKL-induced activation of NF-κB (Fig. 8 D). Accordingly, *Chmp5^Ctsk* osteoclasts displayed an increase in NF-κB DNA-binding activity and a decrease in IκBα levels (Fig. 8, E and F). Blocking this NF-κB activity ablates enhanced activity of TRAP in *Chmp5^Ctsk* osteoclasts, suggesting that aberrant NF-κB signaling is responsible for the phenotypes observed in *Chmp5^Ctsk* osteoclasts (Fig. 8 G). Furthermore, phosphorylation levels of IKKα/β

were relatively normal in *Chmp5^Ctsk* osteoclasts (Fig. 8 F) and CHMP5 overexpression inhibited NF-κB activation by a constitutively active IKKβ, but not by RelA (unpublished data). Thus, these results suggest that CHMP5 functions downstream of the IKK complex and upstream of RelA.

CHMP5 and USP15 dampen RANK–mediated NF-κB activation and osteoclast differentiation via IκBα stabilization

To gain insight into the mechanism by which CHMP5 regulates NF-κB signaling, affinity purification–based mass spectrometry was performed to identify CHMP5-binding proteins. Because CHMP5 interacts with other CHMP family proteins as a component of the endosomal sorting complexes required for transport (ESCRT) machinery (Shim et al., 2006; Tsang et al., 2006), Flag-tagged CHMP5-WT and a CHMP5 mutant (D3) that fails to bind to other CHMP proteins were used to identify non-ESCRT related proteins that are associated with the NF-κB pathway (unpublished data). As expected, ESCRT components, including VPS4B and CHMP1B, 2A, 2B, and 4B, were pulled down by CHMP5-WT but not the CHMP5-D3 mutant. Ingenuity pathway analysis of the CHMP5-binding proteins identified enrichment of the protein ubiquitination pathway including the PDB genetic risk factor VCP/p97 (Yamanaka et al., 2012) and the deubiquitinating enzyme USP15 (Schweitzer et al., 2007; unpublished data). Likewise, size exclusion chromatography showed that endogenous VCP/p97 and USP15 cofractionated with a subset of CHMP5, RelA, IκBα, and the E3 ligase β-Trcp, which is consistent with a previous study showing that VCP/p97 binds ubiquitinated IκBα and β-Trcp (Fig. 8 A; Dai et al., 1998; Li et al., 2014). Furthermore, immunoprecipitation analysis confirmed that both endogenous and overexpressed CHMP5 interact with USP15, VCP/p97, and β-Trcp in an osteoclast line and HEK293 cells, respectively (Fig. 8 H and unpublished data). Thus, in osteoclasts, CHMP5 is a component of the 550-kD protein complex containing a subset of NF-κB RelA/IκBα and binds proteins involved in the regulation of ubiquitin-mediated proteasomal degradation, including VCP/p97, USP15, and β-Trcp (Fig. 8 I).

Given that CHMP5 binds the RelA–IκBα complex alongside USP15, VCP/p97, and β-Trcp, we hypothesized that CHMP5 may regulate NF-κB signaling via modulating ubiquitination of IκBα. An in vitro ubiquitination assay revealed that IκBα ubiquitination was markedly inhibited by overexpression of CHMP5 or USP15 (Fig. 9 A), which is accompanied with pulse-chase labeling experiments showing that IκBα stability was increased by overexpression of CHMP5 or USP15 (Fig. 9, B and C). Accordingly, the ability of RANKL to induce IκBα degradation was enhanced in the absence of CHMP5 or USP15 (Fig. 9, D and E). Thus, CHMP5 and USP15 appear to stabilize IκBα in osteoclasts via suppression of ubiquitination-mediated proteasomal degradation. Given in vitro ubiquitination and deubiquitination assays that either SCF^β-Trcp-mediated ubiquitination of IκBα or ubiquitinated IκBα levels were not affected by addition of recombinant

CHMP5, CHMP5 is unlikely to suppress the IκBα ubiquitination or directly possess deubiquitinating enzyme activity (unpublished data). CHMP5 overexpression did not inhibit RANKL-induced NF-κB activation in the absence of USP15, indicating that CHMP5 requires USP15 to suppress NF-κB signaling downstream of RANKL (Fig. 9 F). In this respect, USP15 overexpression inhibited RANKL-induced NF-κB activation (Fig. 9 G) and USP15 knockdown increased sensitivity of RANKL to osteoclast differentiation (Fig. 9 H). Collectively, these data suggest that the CHMP5–USP15 complex suppresses RANK-mediated NF-κB activation via IκBα stabilization in osteoclasts, in which mechanism it prevents proteasomal degradation of IκBα leading to the retention of NF-κB in an inactive cytosolic complex.

CHMP5 mediates deubiquitination of the VCP/p97 complex via USP15

VCP/p97 is a type II AAA-ATPase that regulates unfolding of proteins as a ubiquitin-selective chaperone, and genetic variants in *VCP* cause inclusion body myopathy associated with Paget's disease of bone and frontotemporal dementia (IBMPFD; Rape et al., 2001; Watts et al., 2004). As it has also been suggested that VCP/p97 regulates ubiquitin-mediated proteasomal degradation of IκBα (Dai et al., 1998), we speculated that VCP/p97 may cooperate with CHMP5 and USP15 to regulate IκBα degradation. To confirm the observation that the CHMP5 complex in osteoclasts contains the deubiquitinating enzyme USP15 and VCP/p97 (Fig. 8, A and I), the physical interactions between CHMP5, USP15, and VCP/p97 were studied using cell-free immunoprecipitation analysis (Fig. 10 A). Intriguingly, CHMP5 interacts directly with both USP15 and VCP/p97, whereas there was no direct interaction between USP15 and VCP/p97. Likewise, in osteoclasts the interaction of USP15 with VCP/p97 was markedly decreased in the absence of CHMP5 (Fig. 10 B), suggesting that CHMP5 mediates the interaction between USP15 and VCP/p97. Previous studies have shown that VCP/p97 and its cofactors interact with ubiquitinated client proteins and facilitate their degradation in proteasome (Koegl et al., 1999; Dai and Li, 2001). We therefore examined the effect of CHMP5 and USP15 on ubiquitination levels of VCP/p97 client proteins using a ubiquitination assay (Fig. 10 C). Similar to our observation that IκBα ubiquitination was suppressed by CHMP5 working together with USP15 (Fig. 9 A), overexpression of CHMP5 or USP15 down-regulated the ubiquitination of proteins physically associated with Myc-VCP/p97. Thus, CHMP5 is likely to dampen ubiquitination of VCP/p97-client proteins via recruitment of USP15 to VCP/p97.

IBMPFD is associated with missense mutations in *VCP/p97*, the majority of which are located in the N-terminal and the D1 ATPase domains (Nalbandian et al., 2011). Among these, R155H has been reported as the most common VCP mutation causing IBMPFD, and A232E is associated with severe clinical manifestations such as early onset of PDB and aggressive myopathy (Watts et al., 2004). To examine if IBMPFD-associated
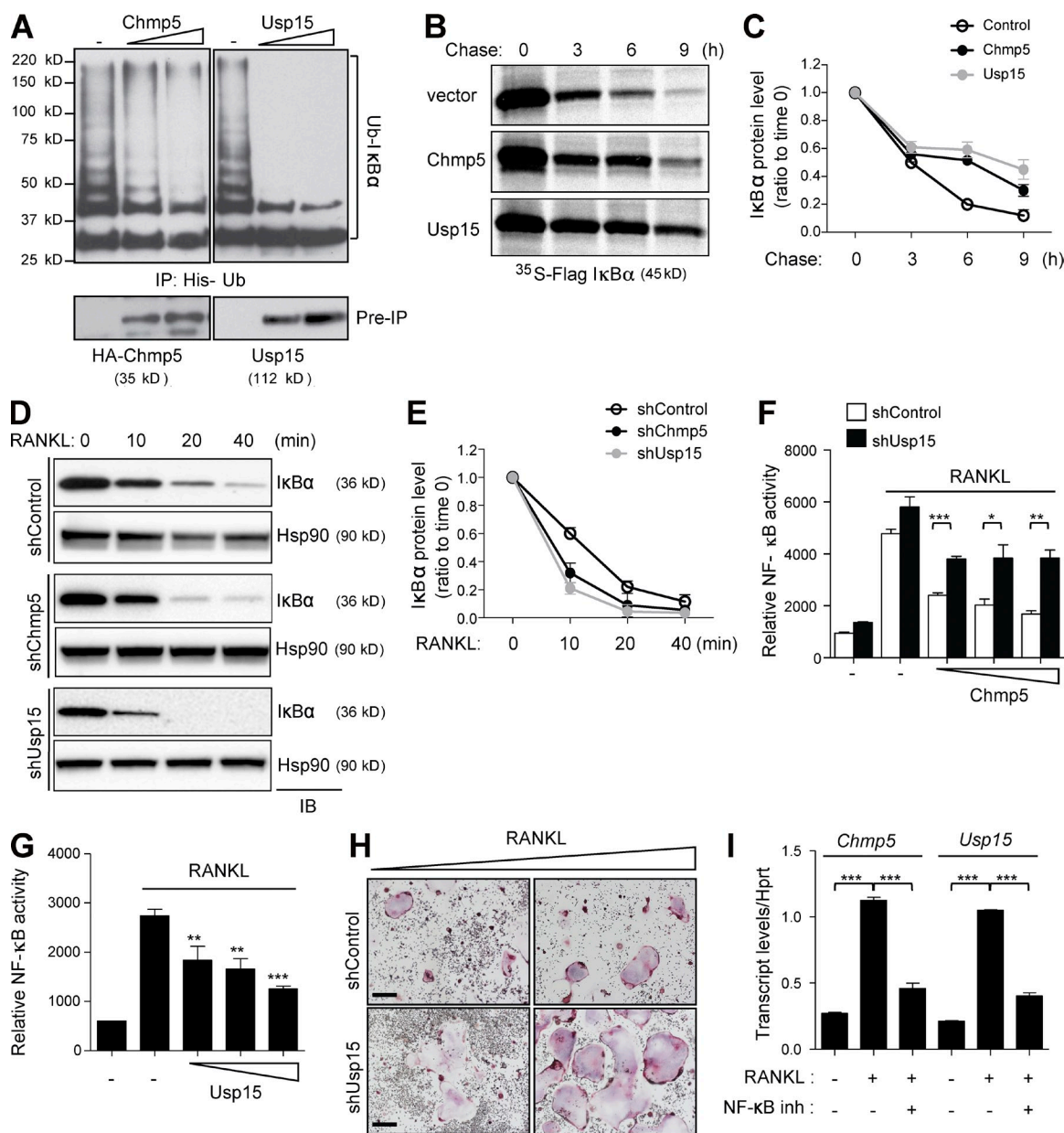
Figure 9. CHMP5 and USP15 suppress RANKL–induced NF–κB activation and osteoclast differentiation via stabilization of IκBα. (A) HEK293 cells were transfected with Chmp5 or Usp15 along with Flag-IκBα, His-ubiquitin, and Myc-β-Trcp, treated with 10 μM MG132, and subjected to IκBα ubiquitination (top) and protein expression assays (bottom). (B and C) HEK293 cells were transfected with control vector, Chmp5, or Usp15 along with Flag-IκBα, and IκBα stability was determined by pulse–chase labeling with [³⁵S]-methionine followed by autoradiography and quantified by ImageJ (C). (D and E) RAW264.7 cells expressing control vector, Chmp5, or Usp15 shRNA were stimulated with 25 ng/ml of RANKL at different time points, and immunoblotted with the indicated antibodies (D). IκBα degradation was quantified using ImageJ and normalized to Hsp90 expression (E). (F and G) RAW264.7 cells expressing control vector or Usp15 shRNA were transfected with Chmp5 along with PBII-luc and *Renilla* (F). Alternatively, RAW264.7 cells were transfected with Usp15 in a dose-dependent manner along with PBII-luc and *Renilla* (G). Luciferase activity was measured and normalized to *Renilla*. *, P < 0.05; **, P < 0.01; ***, P < 0.0001 by a Bonferroni-corrected two-tailed Student's *t* test. (H) RAW264.7 cells expressing control vector or Usp15 shRNA were cultured in the presence of M-CSF and different concentrations of RANKL. TRAP staining was performed after 6 d. (I) WT BMMs were treated with vehicle or NF-κB inhibitor for 1 h before RANKL stimulation. After 48 h of stimulation with RANKL, Chmp5 and Usp15 expression was analyzed by RT-PCR. ***, P < 0.0001 by a Bonferroni-corrected two-tailed Student's *t* test. Data in A–I represent *n* = 3 independent experiments. *, P < 0.05; **, P < 0.01; ***, P < 0.001. Bar: (H) 60 μm.

VCP/p97 mutations alter the binding affinity of VCP/p97 to CHMP5 or USP15, immunoprecipitation analysis was performed with Myc-tagged VCP/p97 R155H and A232E constructs (Fig. 10, D and E). Both VCP/p97 R155H and A232E displayed markedly decreased binding to CHMP5 and USP15. Similarly, whereas CHMP5 or USP15 can suppress the ubiquitination of the client proteins associated with VCP/p97-WT, VCP/p97-R155H, and VCP/p97-A232E were refractory
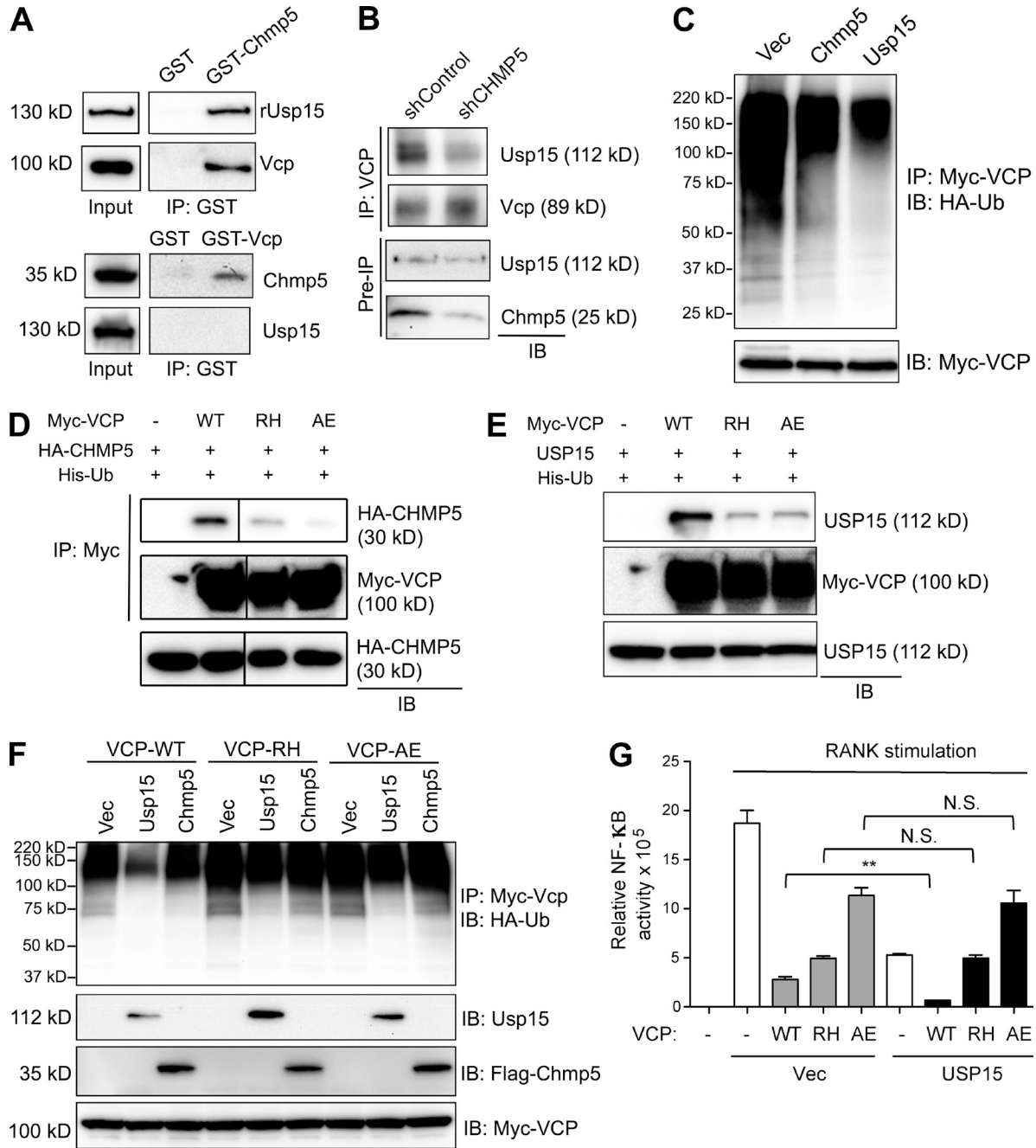
Figure 10. **CHMP5 mediates deubiquitination of the VCP/p97 complex via USP15.** (A) GST or GST-Chmp5 was incubated with the purified proteins, immunoprecipitated with glutathione-agarose, and immunoblotted with the indicated antibodies (top). Alternatively, GST or GST-VCP was incubated with purified CHMP5 protein (bottom). Input indicates loading controls for USP15, VCP, and CHMP5. (B) RAW264.7 cells expressing a control vector or Chmp5 shRNA were cultured with 5 µg of RANKL for 2 d before treatment with 10 µM MG132. Cell lysates were immunoprecipitated with anti-Vcp antibody and protein G–conjugated dynabeads and immunoblotted with the indicated antibodies. (C) HEK293 cells were transfected with Myc-VCP and HA-ubiquitin in the absence or presence of CHMP5 or USP15. 24 h later, cells were treated with 10 µM MG132 and subjected to ubiquitination of Myc-VCP. (D and E) HEK293 cells were transfected with HA-CHMP5 (D) or USP15 (E) and His-ubiquitin along with vector, Myc-VCP (WT), or Myc-VCP mutants (R155H, A232E). 24 h later, cells were treated with 10 µM MG132, immunoprecipitated with anti-Myc antibody–conjugated agarose, and immunoblotted with the indicated antibodies. (F) HEK293 cells were transfected with Myc-VCP (WT) or Myc-VCP mutants (R155H, A232E) and HA-ubiquitin in the absence or presence of CHMP5 or USP15. 24 h later, cells were treated with 10 µM MG132 and subjected to ubiquitination of Myc-VCP. (G) HEK293 cells were transfected with vector, Myc-VCP (WT), or Myc-VCP mutants (R155H, A232E) along with Flag-RANK, PBII-luc and *Renilla* in the absence or presence of USP15, and 24 h later, luciferase activity was measured and normalized to *Renilla*. **, P < 0.01 by a Bonferroni-corrected two-tailed Student's *t* test. Data in A–G represent *n* = 2 independent experiments. **, P < 0.01.

to this effect (Fig. 10 F). Thus, the R155H and A232E mutations disrupt the physical and functional engagement of VCP/p97 with CHMP5 and USP15. Consistent with this engagement with CHMP5 and USP15, expression of VCP/p97-WT but not VCP/p97-R155H or VCP/p97-A232E inhibited RANK-mediated NF-κB activation (Fig. 10 G), and addition of USP15 promoted a further decrease in the presence of VCP/p97-WT but not VCP/p97-R155H or VCP/p97-A232E (Fig. 10 G). Thus, the IBMPFD-associated VCP/p97 mutations that disrupt engagement with CHMP5 and USP15 also influence the ability of VCP/97 to regulate the activation of NF-κB by RANK.

DISCUSSION

Our data reveal that CHMP5 is a key dampener of bone remodeling, preventing the development of a high turnover PDB-like state. CHMP5 mobilizes USP15 to deubiquitinate and stabilize IκBα, inhibiting ubiquitin-dependent proteasomal degradation. This dampens RANK-mediated activation of NF-κB in osteoclasts, in turn increasing the threshold of stimulation required for osteoclast differentiation and osteoclast-mediated bone resorption. Intriguingly, CHMP5 and USP15 expression are both up-regulated by RANKL, suggesting that they may function in concert as a negative feedback mechanism to suppress NF-κB activity (Fig. 9 I).

The rescue of the $Chmp5^{Ctsk}$ bone phenotype by $Rank$ haploinsufficiency demonstrates that exaggerated bone remodeling observed in vivo is directly attributable to the enhanced sensitivity to RANK stimulation observed in osteoclasts in vitro, though this result does not exclude that alterations in other pathways may also contribute to the phenotype observed. Notably, $Rank$ heterozygous mice do not display detectable alterations in basal osteoclast numbers or activity (Dougall et al., 1999). Thus, the ability of CHMP5 deletion to increase the sensitivity of osteoclasts to RANK stimulation in vitro is supported by the observation that $Chmp5^{Ctsk}$ mice also display an increased sensitivity to reductions in $Rank$ gene dosage in vivo. This conclusion is also reinforced by the observation that OPG-Fc, which directly inhibits RANK activation, is highly effective in rescue of the $Chmp5^{Ctsk}$ bone phenotype. Unlike OPG-Fc treatment, $Chmp5^{Ctsk}$ mice treated with bisphosphonates, which suppress osteoclast resorptive activity without directly affecting activation of RANK, still display bone expansion as a result of incomplete blockade of osteoblast activity. Through comparison of these attempts to reverse the $Chmp5^{Ctsk}$ bone phenotype, we conclude that the osteoclast/osteoblast coupling in $Chmp5^{Ctsk}$ mice is RANK-dependent but is largely independent of osteoclast resorptive activity. Thus, coupling factors relevant to this model are likely to be directly produced by osteoclasts as opposed to being growth factors liberated from the bone matrix during osteoclast-mediated bone resorption. Consistent with this model, $Chmp5^{Ctsk}$ osteoclasts display an enhanced ability to promote osteoblast activity in a co-culture system in vitro. Likewise, transcriptome analysis of $Chmp5^{Ctsk}$ osteoclasts

demonstrates that CHMP5 not only suppresses osteoclast differentiation, but it also suppresses a broad transcriptional program driving the expression of several osteoclast/osteoblast coupling factors. Among these coupling factors whose expression is regulated by CHMP5, the EphrinB2–EphB4 pathway is particularly important, as it is necessary for the enhanced coupling activity of CHMP5-deficient osteoclasts. However, the observation that several known osteoclast/osteoblast coupling factors are regulated by CHMP5 indicates that additional pathways also contribute to this phenotype. Thus, by acting as a rheostat to tune RANK signaling in osteoclasts, CHMP5 in turn regulates systemic coupling of osteoclast and osteoblast activity.

Our previous study of mice with germline deletion of $Chmp5$ indicated the importance of CHMP5 function in late endosomal trafficking to lysosomes and in TGFβ signaling via regulating the lysosomal degradation of TGFβ receptors (Shim et al., 2006). However, lysosomal biogenesis and endosomal structures are largely intact in $Chmp5^{Ctsk}$ osteoclasts and TGFβ receptor levels and TGFβ–induced SMAD activation were unaltered in the absence of CHMP5 (unpublished data). This may be due to Ctsk-cre deleting $Chmp5$ after lysosomal biogenesis is complete in osteoclasts, or the specialization of endosomal/lysosomal structures in osteoclasts may necessitate the use of different pathways for their biogenesis. Additionally, we found that distinct domains mediate the interactions of CHMP5 with the endocytic and NF-κB pathways, implying that functions of CHMP5 in regulating NF-κB activity are biochemically distinct from its role in lysosomal biogenesis in osteoclasts. However, further studies will be required to determine if the functions of CHMP5 to regulate endocytosis and NF-κB pathway are linked.

The spectrum of human PDB and related monogenic forms of PDB encompass a wide range of phenotypic variation (Daroszewska and Ralston, 2006). In this respect, the phenotype of $Chmp5^{Ctsk}$ mice fits clearly within this spectrum, as the combination of periosteal hyperdynamic bone deposition, exaggerated bone remodeling coupled with increased activities of osteoclasts and osteoblasts, bone expansion, and osteoclasts displaying increased numbers of nuclei are pathognomonic for Paget's-spectrum disorders. Although sporadic PDB displays a greatly increased relative risk of osteosarcoma formation (Hansen et al., 2006), no osteosarcomas were observed over the course of this study, and the early onset and polyostotic nature of the $Chmp5^{Ctsk}$ bone phenotype is markedly different from classical PDB. Some PBD patients have been observed to display marrow fibrosis (Murrin and Harrison, 2004), and this is not observed in $Chmp5^{Ctsk}$ mice. Similarly, the vascular calcifications associated with JPD are not observed in $Chmp5^{Ctsk}$ mice (Saki et al., 2013; Whyte et al., 2014). However, further studies will be required to determine the reasons for these differences. Lastly, it is possible that environmental factors are needed for full penetrance of all aspects of PDB phenotypes, as environmental factors which are acknowledged to be especially important for the pathogenesis of PDB (Roodman, 2010).

Given that variants in *CHMP5* gene have yet to be identified in human patients with a Paget's spectrum disorder, we instead considered whether CHMP5 displays a functional interaction with other known genes implicated in a Paget's spectrum disorder. As variants in *VCP/p97* gene cause the Paget's–related disorder IBMPFD, and VCP/p97 has been implicated in regulation of IκBα, the relationship between CHMP5 and VCP/p97 was studied, demonstrating that CHMP5 serves as an adaptor to recruit the deubiquitinating enzyme USP15 to the VCP/p97 complex. This recruitment then leads to USP15-mediated deubiquination of VCP/p97 client proteins, likely salvaging them from proteasomal degradation. Accordingly, mutations in VCP/p97 that cause IBMPFD (R155H and A232E) disrupt both the physical and functional interaction with CHMP5 and USP15. Collectively with the PDB-like skeletal phenotype of *Chmp5^Ctsk* mice, this indicates that CHMP5 cooperates with VCP/p97 to regulate RANK signaling and that disruption of this functional interaction may be a key factor in the development of some Paget's spectrum disorders. This also raises the possibility that VCP/p97 serves an important function to select the substrates targeted by the CHMP5–USP15 complex for deubiquitination.

The exuberant bone formation and expansion seen in *Chmp5^Ctsk* mice demonstrates the importance of CHMP5 for the regulation of bone turnover rates. As, to our knowledge, *Chmp5^Ctsk* mice represent one of the most severe mouse models of high turnover metabolic bone disease yet reported, we believe that they may offer an opportunity to identify osteoclast/osteoblast coupling factors with anabolic activity, which may ultimately have utility for the treatment of osteoporosis. Additionally, the early onset, high severity, and complete penetrance displayed by this model may make this an attractive preclinical model to validate treatment for Paget's-spectrum disorders.

MATERIALS AND METHODS

Materials. Mouse M-CSF and mouse RANKL were purchased from R&D Systems. Antibodies to Chmp5 (Santa Cruz Biotechnology, Inc.), Hsp90α/β (Santa Cruz Biotechnology, Inc.), IκBα (Santa Cruz Biotechnology, Inc.), Ubiquitin (Santa Cruz Biotechnology, Inc.), β-Trcp/HOS (Santa Cruz Biotechnology, Inc.), NF-κB/p50 (Santa Cruz Biotechnology, Inc.), anti-HA HRP conjugated antibody (Santa Cruz Biotechnology, Inc.), p65/RelA (Enzo Life Sciences), NF-κB/p100 (Cell Signaling Technology), Vcp/p97 (Cell Signaling Technology), Flag (Sigma-Aldrich), GFP (Clontec), GAPDH (Affinity Bioreagents), Usp15 (Bethyl Laboratories), Nfatc1 (BioLegend), phospho-IKKα/β (Cell Signaling Technology), Bi-phospho-Syk (Y525/526; Abgent), TGF-β receptor, type 1 (EMD Millipore), phospho-Src Family (Tyr416; Cell Signaling Technology), and Cathepsin K (Biovision) were used for immunoblotting. Anti-HA agarose-conjugated antibody (Santa Cruz Biotechnology, Inc.) and anti–c-Myc HRP-conjugated antibody (Santa Cruz Biotechnology, Inc.), and anti-HA HRP–conjugated antibody were used for immunoprecipitation. NF-κB inhibitor Bay 11–7035 and active Rac1 detection kit were purchased from Santa Cruz Biotechnology, Inc. and Cell Signaling Technology, respectively. For recombinant proteins, GST-NF-κB p65 and GST-IκBα were purchased from Enzo Life Sciences, and GST-CHMP5 and GST-p97/VCP were purchased from Novus Biologicals. The recombinant active SCF-Skp2 protein complex and activated IκBα were purchased from EMD Millipore.

Mice. To generate *Chmp5* floxed mice, exon 4 and 5 flanked by a 5′ loxP site and a 3′ loxP-PGKNEO-loxP cassette was cloned into the pEasy–flox vector and the ES clones with homologous recombination were selected by neomycin and validated by Southern blotting. Subsequently, Cre recombinase-expressing construct was transfected into the validated neomycin-resistant clones and further selected to delete the PGK-NEO cassette. Mice bearing the targeted allele were generated by blastocyst injection and backcrossed with C57BL/8 mice up to F8 generation.

Chmp5^Ctsk mice were generated by intercrossing *Chmp5^fl/+;*Cathepsin K-Cre breeders with *Chmp5^fl/fl* mice. Cathepsin K-cre mice were a gift from S. Kato (University of Tokyo, Tokyo, Japan). *Chmp5^Ctsk/Rank^het* mice were generated by intercrossing *Chmp5^fl/+;Rank^fl/+;*Cathepsin K-Cre mice with *Chmp5^fl/fl;Rank^fl/+* breeders. All mice were on a C57BL/6 background. All animals were maintained in accordance with the National Institutes of Health Guide for the Care and Use of Laboratory Animals and were handled according to protocols approved by the Weill Cornell Medical College subcommittee on animal care (IACUC).

Cell culture, osteoclast, and osteoblast differentiation. Primary BMMs and RAW264.7 cells (American Type Culture Collection) were cultured in α-minimum essential medium (CellGro) supplemented with 10% FBS (Hyclone), 1% penicillin/streptomycin (Invitrogen), and 2 mM L-glutamine (Invitrogen) in 5% CO_2 at 37°C. Primary calvarial osteoblasts (COBs) and BM-derived stromal cell (BMSCs) were cultured in α-MEM (α-MEM; Invitrogen) containing 10% FBS, 1% penicillin/streptomycin, 2 mM L-glutamine, 1% Hepes, and 1% nonessential amino acids. For osteoblast differentiation, the cells were cultured under basal medium containing β-glycero-phosphate and α-ascorbic acid.

For osteoclast differentiation analysis, the femur and tibia were carefully dissected from 6-wk-old male *Chmp5^fl/fl* and *Chmp5^Ctsk* mice, and BM cells collected by flushing were plated overnight in α−MEM plus 10% FBS. Nonadherent cells were collected and seeded on a 100-mm dish with mM-CSF (30 ng/ml, R&D Systems). After 48 h, nonadherent cells were discarded and adherent cells were used as BMMs. BMMs were detached from the 100-mm dish using Detachin (Genlantis). For the osteoclastogenesis, RAW264.7 (2.6 × 10^4 cells/cm²) cells and BMMs (5.2 × 10^4 cells/cm²) were cultured for 6 d in α−MEM containing 5 ng/ml mRANKL (R&D Systems) or 20 ng/ml mRANKL and 40 ng/ml mM-CSF, respectively. Alternatively, cells were plated on the bovine cortical bone slices (boneslices.com) and cultured with 20 ng/ml mRANKL and 40 ng/ml mM-CSF. The number and area of the resorptive pits on the bone slice were counted and the amount of CTX liberated from the bone slice to medium was measured by an ELISA kit (IDS) to assess bone resorption activity.

Osteoblast culture with osteoclast–conditioned medium. The conditioned medium of *Chmp5^fl/fl* and *Chmp5^Ctsk* osteoclasts was harvested as described previously. (Matsuoka et al., 2014) In brief, after 1 or 2 d culture with α-MEM medium containing 10% FBS, mRANKL (20 ng/ml), and mM-CSF (40 ng/ml), *Chmp5^fl/fl* and *Chmp5^Ctsk* BMMs were cultured in the conditioned medium (CM) for 1 or 2 d and CM was harvested. Each CM was concentrated using the Amicon Ultra-15 Filter Unit (10K; EMD Millipore). Co-culture of osteoblasts with *Chmp5^fl/fl* and *Chmp5^Ctsk* osteoclasts was performed in the presence of various concentrations of mouse-Fc or mouse EphB4-Fc (R&D Systems). After 12–18 d of culture, osteoblasts were stained with alizarin red and mineralization activity was measured by colorimetric analysis.

Histology, immunohistochemistry, and in situ hybridization. For histological analysis, hindlimbs were dissected from 6- or 12-wk-old male mice, fixed in 10% neutral buffered formalin for 24–48 h, and decalcified by daily changes of 15% tetrasodium EDTA for 2 wk. Tissues were dehydrated by passage through an ethanol series, cleared twice in xylene, embedded in paraffin, and sectioned at 7 μm thickness along the coronal plate from anterior to posterior. Decalcified femoral sections were stained with hematoxylin and eosin (H&E), Safranin O, and tartrate–resistant acid phosphatase (TRAP).

For in situ hybridization, DIG-labeled probes were prepared to detect type I collagen (Col1) and osteocalcin (Ocn) mRNA expression using the DIG-labeling kit (Roche) according to the manufacturer's instructions. Paraffin sections were dewaxed and quenched with endogenous peroxidase, and

1298

Role for CHMP5 in NF-κB signaling and bone turnover | Greenblatt et al.

then hybridized with the probes. DIG-labeled probe was then detected by immunostaining with anti–DIG-POD and streptavidin-HRP.

For immunohistochemistry, paraffin tissue sections were dewaxed and blocked with 3% goat serum, 1% BSA, 0.1% Triton X-100 in PBS for 1 h at room temperature. Sections were incubated with antibodies specific to CHMP5 (Santa Cruz Biotechnology, Inc.; clone H7), PECAM-1 (CD31, Santa Cruz Biotechnology, Inc.; clone M6), VEGF (EMD Millipore, 07–1420), and collagen type I (Rockland) at 4°C overnight, treated with TSA-biotin (Perkin Elmer), and streptavidin-HRP, as per manufacturer's instructions, and then visualized with 2,2′-diaminobenzidine tetrahydrochloride.

μCT analysis, bone histomorphometry, and skeletal preparation. For μCT analysis, a Scanco Medical μCT 35 system with an isotropic voxel size of 7 μm was used to image the distal femur. Scans were conducted in 70% ethanol and used an x-ray tube potential of 55 kVp, an x-ray intensity of 0.145 mA, and an integration time of 600 ms. For trabecular bone analysis of the distal femur, a upper 2.1-mm region beginning 280 μm proximal to the growth plate was contoured. For cortical bone analysis of femur and tibia, a midshaft region of 0.6 mm in length was used. Trabecular and cortical bones were thresholded at 211 and 350 per mgHA/cm^3, respectively. μCT CT scans of skulls, vertebrae and feet were performed using isotropic voxel sizes of 12 and 20 μm. 3D images were obtained from contoured 2D images by methods based on distance transformation of the binarized images. All images presented are representative of the respective genotypes.

For the bone histomorphometry, 20 mg/kg calcein (Sigma-Aldrich) and 30 mg/kg demeclocycline (Sigma-Aldrich) dissolved in 2% sodium bicarbonate solution were injected subcutaneously with 4-d interval at day 6 and day 2 before the sacrifice. Undecalcified tibia samples were fixed in 4% PFA embedded in plastic resin for bone sections. The sections were stained with von Kossa and TRAP, and numbers and activities of osteoblasts and osteoclasts were quantified using the Bioquant Osteo Image Analysis System.

Skeletons were also prepared for analysis of gross morphology using the method of McLeod. In brief, mice were sacrificed, skinned, eviscerated, and fixed in 95% ethanol for a day. Next, skeletons were stained by Alizarin Red S and Alcian Blue solutions and sequentially cleared in 1% potassium hydroxide.

Complete blood count test. Blood was collected from 12-wk-old male *Chmp5$^{fl/fl}$* and *Chmp5^{Ctsk}* mice (*n* = 5 mice/group) by cardiac puncture immediately after sacrifice. All parameters for complete blood counts were calculated by a Hemavet 950 analyzer (Drew Scientific) according to the manufacturer's instructions.

Antiresorptive treatment. PBS, 2.5 mg/kg alendronate sodium trihydrate (Sigma-Aldrich), 100 μg/kg zolendronic acid monohydrate (Sigma-Aldrich), or rat 3 mg/kg OPG–Fc (Amgen Inc.) was intraperitoneally injected weekly to *Chmp5$^{fl/fl}$* and *Chmp5^{Ctsk}* male mice from 2–5 wk of age, and the mice were all sacrificed at 6 wk of age and used for skeletal analysis.

Bone RNA isolation and RT-PCR analysis. Bone RNA was prepared as previously described. In brief, tibias were isolated from 6-wk-old male *Chmp5$^{fl/fl}$* and *Chmp5^{Ctsk}* mice, and cleaned of surrounding soft tissue, and BM cells were removed by flushing with PBS. Immediately, bones were transferred to the prechilled tubes containing QIAzol lysis reagent (QIAGEN) and homogenized using a Polytron (Kinematic PT 2100, 7 mm tip) under a rack surrounded by liquid nitrogen. cDNA was reverse transcribed using random primers and MultiScribe reverse transcription (Applied Biosystems) and used in real-time PCR with a SYBR Green PCR Master Mix kit (Applied Biosystems). The specific primer pairs are shown in Table S1.

RNA–sequencing analysis and gene set enrichment analysis (GSEA). BMMs were isolated from male *Chmp5$^{fl/fl}$* and *Chmp5^{Ctsk}* mice (*n* = 3 mice per group) and cultured in the presence of M-CSF and RANKL. Total RNAs were isolated from osteoclasts at day 3 of culture using QIAzol lysis reagent (QIAGEN). Quality control test of the RNAs were conducted using the Agilent Bioanalyzer 2100 and libraries for Illumina sequencing were

prepared as described. After ligation of Illumina PE adaptors, cDNA was separated by electrophoresis through agarose gels and fragments with a size of 300–350 base pairs were excised for analysis. 50 bases, pair-end read sequencing was performed on the Illumina HiSeq2000, which yielded 74 × 10^6 to 92 × 10^6 paired-end raw reads per sample. Those reads were aligned to the mouse genome (*Mus musculus* UCSC mm10) using with TopHat software (version 2.0.10). Differentially expressed genes were presented using hypergeometric calculation implemented in the DESeq Bioconductor package in R statistical language.

Gene sets from the Broad Institute Molecular Signatures Database and a modified gene set (Table S2) were used, and multiple lists of enriched gene sets were generated using the GSEA algorithm as previously described. Enrichment for up-regulation or down-regulation in *Chmp5^{Ctsk}* RNAs was assessed against a gene list preranked for log$_2$ ratio of expression from *Chmp5^{Ctsk}* RNAs to expression from *Chmp5$^{fl/fl}$* RNAs.

Immunoprecipitation, immunoblotting, immunofluorescence, and pulse–chase analysis. HEK293T cells were transfected with the indicated DNA constructs using Effectene reagents (QIAGEN), and then lysed in TNT lysis buffer (10 mM Tris, 50 mM NaCl, 5 mM EDTA, 2 mM NaF, 30 mM sodium pyrophosphate, 100 mM Na$_3$VO$_4$, 0.5 mM PMSF, 1 μg/ml leupeptin, 5 μg/ml aprotinin, and 1% Triton X-100). Proteins from cell lysates were immunoprecipitated with Flag-, HA-, or Myc-conjugated agarose, and the immunoprecipitates were subjected to SDS-PAGE and transferred to Immunobilon-P membranes (EMD Millipore). Alternatively, *Chmp5$^{fl/fl}$* and *Chmp5^{Ctsk}* BMMs were cultured in the presence of M-CSF and RANKL, and after 3–4 d total cell lysates were immunoblotted with antibodies specific to IκBα, SRC, phospho-SRC, phospho-SYK, and CHMP5. Immunoblotting with antibodies specific to Gapdh or Hsp90α/β was used as a loading control. For actin ring staining, cells were fixed in 4% paraformaldehyde and permeabilized in 0.1% Triton X-100, washed in PBS, and stained with Alexa Fluor 488-phalloidin (Life Technologies).

HEK293 cells transfected with the indicated DNA constructs were incubated under starvation conditions (3% dFBS, glutamine and Hepes in Cys/Met free DMEM) for 3 h. Subsequently, cells were incubated in labeling medium containing [^{35}S]-methionine for 1 h, and cultured in chase medium (5% FBS, +Cys, +Met, glutamine, and Hepes in DMEM) for various durations. Cells were then lysed, immunoprecipitated with anti-Flag (M2) antibody–conjugated agarose, and subjected to SDS-PAGE. Labeled proteins were visualized with autoradiography and were quantified using ImageJ (National Institutes of Health).

Luciferase reporter assay and DNA binding assay. In brief, HEK293 cells or RAW264.7 cells were transfected with a NF-κB–responsive (PBII-luc) or AP1-responsive reporter gene (2xAP1-luc) along with *Renilla* (Promega). 24 h after transfection, the cells were stimulated with 50 ng/ml RANKL for 48 h and lysed with 1× passive lysis buffer (Promega). Luciferase activity was measured using the dual-luciferase reporter assay kit (Promega). Relative luciferase activity was normalized to *Renilla*.

NF-κB DNA binding assays were performed as described in the manufacturer's instructions for the NF-κB p65 enzyme linked immunosorbent assay (ELISA) kit (Enzo Life Sciences). In brief, total cell lysates were incubated for 30 min at room temperature on the p65 consensus oligonucleotide-coated plates. The active form of p65 bound to consensus oligonucleotides were sequentially incubated with anti-p65 antibody and HRP-conjugated secondary antibody. The oligonucleotide-bound active p65 were incubated with a chemiluminescent substrate, and DNA binding affinity was measured by a luminometer.

Ubiquitination assay. HEK293 cells were transfected with His–ubiquitin, Myc-β-Trcp, and Flag-IκBα, along with control vector, CHMP5, or USP15. After 24-h transfection, the cells were treated with 10 mM MG132 (EMD Millipore) for 6 h, lysed and sonicated in the denaturation buffer (8 M Urea, 50 mM Tris, pH 8.0, 1.0% Triton X-100, 10 mM Imidazol, and 10 mM β-mercaptoethanol), and immunoprecipitated with Ni-NTA beads.

The immunoprecipitates were subjected to SDS-PAGE and immunoblotted with anti-IκBα antibody. Alternatively, RAW264.7 cells were infected with lentiviruses expressing control (GFP and Luciferase genes; Broad Institute, Boston, MA), mouse Chmp5 (Sigma-Aldrich), or mouse Usp15 (Sigma-Aldrich) shRNAs, and the cells were treated with 10 mM MG132 for 8 h before 1-h RANKL stimulation. The cells were lysed, immunoprecipitated with anti-IκBα and protein G–agarose, subjected to SDS-PAGE, and immunoblotted with anti-ubiquitin antibody.

Biomarkers of bone turnover. Blood was collected from 6-wk-old male *Chmp5*$^{fl/fl}$ and *Chmp5*^{Ctsk} mice ($n = 5$/group) by cardiac puncture and divided into two groups. Serum was separated using serum separator tubes and serum levels of ALP (Cloud-Clone), P1NP (IDS), and CTX (IDS) were measured using each ELISA kits as per the manufacturer's instructions.

Statistical analysis. Data are shown as the mean ± SEM. Sample sizes were calculated on the assumption that a 30% difference in the parameters measured would be considered biologically significant with an estimate of sigma of 10–20% of the expected mean. α and β were set to the standard values of 0.05 and 0.8, respectively. No animals or samples were excluded from analysis. In Fig. 4 (f and g), mice were randomized to treatment groups (aldendronate, zolendronate, OPG-Fc, or PBS). μCT analysis was performed in a blinded fashion. We first performed the Shapiro-Wilk normality test for checking normal distributions of the groups. If normality tests passed, two-tailed, unpaired Student's *t* tests were used for the comparisons between two groups; if normality tests failed, Mann-Whitney tests were used for the comparisons between two groups. For the comparisons of three or four groups, we used one-way ANOVA if normality tests passed, followed by Tukey`s multiple comparison test for all pairs of groups. If normality tests failed, Kruskal-Wallis test was performed and followed by Dunn`s multiple comparison test. The GraphPad PRISM software (v6.0a) was used for statistical analysis. P < 0.05 was considered statistically significant. *, P < 0.05; **, P < 0.01; ***, P < 0.001.

Online supplemental material. Table S1 shows the specific primer pairs used in RT-PCR analysis of bone and cultured osteoclast RNAs. Table S2 shows a gene set related to the osteoclast differentiation and fusion modified from Broad Institute Molecular Signatures Database. Online supplemental material is available at http://www.jem.org/cgi/content/full/jem.20150407/DC1.

REFERENCES

Albagha, O.M., M.R. Visconti, N. Alonso, A.L. Langston, T. Cundy, R. Dargie, M.G. Dunlop, W.D. Fraser, M.J. Hooper, G. Isaia, et al. 2010. Genome-wide association study identifies variants at CSF1, OPTN and TNFRSF11A as genetic risk factors for Paget's disease of bone. *Nat. Genet.* 42:520–524. http://dx.doi.org/10.1038/ng.562

Albagha, O.M., S.E. Wani, M.R. Visconti, N. Alonso, K. Goodman, M.L. Brandi, T. Cundy, P.Y. Chung, R. Dargie, J.P. Devogelaer, et al. Genetic Determinants of Paget's Disease (GDPD) Consortium. 2011. Genome-wide association identifies three new susceptibility loci for Paget's disease of bone. *Nat. Genet.* 43:685–689. http://dx.doi.org/10.1038/ng.845

Babst, M., D.J. Katzmann, E.J. Estepa-Sabal, T. Meerloo, and S.D. Emr. 2002. Escrt-III: an endosome-associated heterooligomeric protein complex required for mvb sorting. *Dev. Cell.* 3:271–282. http://dx.doi.org/10.1016/S1534-5807(02)00220-4

Bakwin, H., and M.S. Eiger. 1956. Fragile bones and macrocranium. *J. Pediatr.* 49:558–564. http://dx.doi.org/10.1016/S0022-3476(56)80143-1

Chakravorty, N.K. 1978. Some unusual features of Paget's disease of bone. *Gerontology.* 24:459–472. http://dx.doi.org/10.1159/000212286

Chiu, W.S., J.F. McManus, A.J. Notini, A.I. Cassady, J.D. Zajac, and R.A. Davey. 2004. Transgenic mice that express Cre recombinase in osteo-clasts. *Genesis.* 39:178–185. http://dx.doi.org/10.1002/gene.20041

Cornish, J., K.E. Callon, S.G. Edgar, and I.R. Reid. 1997. Leukemia inhibitory factor is mitogenic to osteoblasts. *Bone.* 21:243–247. http://dx.doi.org/10.1016/S8756-3282(97)00144-0

Cundy, T., L. Wheadon, and A. King. 2004. Treatment of idiopathic hyper-phosphatasia with intensive bisphosphonate therapy. *J. Bone Miner. Res.* 19:703–711. http://dx.doi.org/10.1359/jbmr.040127

Cundy, T., J. Davidson, M.D. Rutland, C. Stewart, and A.M. DePaoli. 2005. Recombinant osteoprotegerin for juvenile Paget's disease. *N. Engl. J. Med.* 353:918–923. http://dx.doi.org/10.1056/NEJMoa050893

Dai, R.M., and C.C. Li. 2001. Valosin-containing protein is a multi-ubiquitin chain-targeting factor required in ubiquitin-proteasome degradation. *Nat. Cell Biol.* 3:740–744. http://dx.doi.org/10.1038/35087056

Dai, R.M., E. Chen, D.L. Longo, C.M. Gorbea, and C.C. Li. 1998. Involvement of valosin-containing protein, an ATPase Co-purified with IkappaBalpha and 26 S proteasome, in ubiquitin-proteasome-mediated degradation of IkappaBalpha. *J. Biol. Chem.* 273:3562–3573. http://dx.doi.org/10.1074/jbc.273.6.3562

Daroszewska, A., and S.H. Ralston. 2006. Mechanisms of disease: genetics of Paget's disease of bone and related disorders. *Nat. Clin. Pract. Rheumatol.* 2:270–277. http://dx.doi.org/10.1038/ncprheum0172

Deckers, M.M., M. Karperien, C. van der Bent, T. Yamashita, S.E. Papapoulos, and C.W. Löwik. 2000. Expression of vascular endothelial growth factors and their receptors during osteoblast differentiation. *Endocrinology.* 141:1667–1674. http://dx.doi.org/10.1210/endo.141.5.7458

Dougall, W.C., M. Glaccum, K. Charrier, K. Rohrbach, K. Brasel, T. De Smedt, E. Daro, J. Smith, M.E. Tometsko, C.R. Maliszewski, et al. 1999. RANK is essential for osteoclast and lymph node development. *Genes Dev.* 13:2412–2424. http://dx.doi.org/10.1101/gad.13.18.2412

Galson, D.L., and G.D. Roodman. 2014. Pathobiology of Paget's disease of bone. *J Bone Metab.* 21:85–98. http://dx.doi.org/10.11005/jbm.2014.21.2.85

Hansen, M.F., M. Seton, and A. Merchant. 2006. Osteosarcoma in Paget's disease of bone. *J. Bone Miner. Res.* **21**(S2, Suppl 2):58–63. http://dx.doi.org/10.1359/jbmr.06s211

Hoyland, J.A., A.J. Freemont, and P.T. Sharpe. 1994. Interleukin-6, IL-6 receptor, and IL-6 nuclear factor gene expression in Paget's disease. *J. Bone Miner. Res.* 9:75–80. http://dx.doi.org/10.1002/jbmr.5650090111

Izawa, T., W. Zou, J.C. Chappel, J.W. Ashley, X. Feng, and S.L. Teitelbaum. 2012. c-Src links a RANK/αvβ3 integrin complex to the osteoclast cytoskeleton. *Mol. Cell. Biol.* 32:2943–2953. http://dx.doi.org/10.1128/MCB.00077-12

Jimi, E., K. Aoki, H. Saito, F. D'Acquisto, M.J. May, I. Nakamura, T. Sudo, T. Kojima, F. Okamoto, H. Fukushima, et al. 2004. Selective inhibition of NF-kappa B blocks osteoclastogenesis and prevents inflammatory bone destruction in vivo. *Nat. Med.* 10:617–624. http://dx.doi.org/10.1038/nm1054

Koegl, M., T. Hoppe, S. Schlenker, H.D. Ulrich, T.U. Mayer, and S. Jentsch. 1999. A novel ubiquitination factor, E4, is involved in multiubiquitin chain assembly. *Cell.* 96:635–644. http://dx.doi.org/10.1016/S0092-8674(00)80574-7

Köhler, J.R. 2003. Mos10 (Vps60) is required for normal filament maturation in *Saccharomyces cerevisiae*. *Mol. Microbiol.* 49:1267–1285. http://dx.doi.org/10.1046/j.1365-2958.2003.03556.x

Kurihara, N., Y. Hiruma, K. Yamana, L. Michou, C. Rousseau, J. Morissette, D.L. Galson, J. Teramachi, H. Zhou, D.W. Dempster, et al. 2011. Contributions of the measles virus nucleocapsid gene and the SQSTM1/p62(P392L) mutation to Paget's disease. *Cell Metab.* 13:23–34. http://dx.doi.org/10.1016/j.cmet.2010.12.002

Li, J.M., H. Wu, W. Zhang, M.R. Blackburn, and J. Jin. 2014. The p97-UFD1L-NPL4 protein complex mediates cytokine-induced IκBα proteolysis. *Mol. Cell. Biol.* 34:335–347. http://dx.doi.org/10.1128/MCB.01190-13

Matsuoka, K., K.A. Park, M. Ito, K. Ikeda, and S. Takeshita. 2014. Osteoclast-derived complement component 3a stimulates osteoblast differentiation. *J. Bone Miner. Res.* 29:1522–1530. http://dx.doi.org/10.1002/jbmr.2187

Murrin, R.J., and P. Harrison. 2004. Abnormal osteoclasts and bone marrow fibrosis in Paget's disease of the bone. *Br. J. Haematol.* 124:3. http://dx.doi.org/10.1046/j.1365-2141.2003.04570.x

Nalbandian, A., S. Donkervoort, E. Dec, M. Badadani, V. Katheria, P. Rana, C. Nguyen, J. Mukherjee, V. Caiozzo, B. Martin, et al. 2011. The multiple faces of valosin-containing protein-associated diseases: inclusion body myopathy with Paget's disease of bone, frontotemporal dementia, and amyotrophic lateral sclerosis. *J. Mol. Neurosci.* 45:522–531. http://dx.doi.org/10.1007/s12031-011-9627-y

Naot, D., U. Bava, B. Matthews, K.E. Callon, G.D. Gamble, M. Black, S. Song, R.P. Pitto, T. Cundy, J. Cornish, and I.R. Reid. 2007. Differential gene expression in cultured osteoblasts and bone marrow stromal cells from patients with Paget's disease of bone. *J. Bone Miner. Res.* 22:298–309. http://dx.doi.org/10.1359/jbmr.061108

Novack, D.V. 2011. Role of NF-κB in the skeleton. *Cell Res.* 21:169–182. http://dx.doi.org/10.1038/cr.2010.159

Ota, K., P. Quint, M. Ruan, L. Pederson, J.J. Westendorf, S. Khosla, and M.J. Oursler. 2013. TGF-β induces Wnt10b in osteoclasts from female mice to enhance coupling to osteoblasts. *Endocrinology.* 154:3745–3752. http://dx.doi.org/10.1210/en.2013-1272

Polyzos, S.A., P.N. Singhellakis, D. Naot, F. Adamidou, F.C. Malandrinou, A.D. Anastasilakis, V. Polymerou, and M. Kita. 2014. Denosumab treatment for juvenile Paget's disease: results from two adult patients with osteoprotegerin deficiency ("Balkan" mutation in the TNFRSF11B gene). *J. Clin. Endocrinol. Metab.* 99:703–707. http://dx.doi.org/10.1210/jc.2013-3762

Raiborg, C., and H. Stenmark. 2009. The ESCRT machinery in endosomal sorting of ubiquitylated membrane proteins. *Nature.* 458:445–452. http://dx.doi.org/10.1038/nature07961

Ralston, S.H., A.L. Langston, and I.R. Reid. 2008. Pathogenesis and management of Paget's disease of bone. *Lancet.* 372:155–163. http://dx.doi.org/10.1016/S0140-6736(08)61035-1

Rape, M., T. Hoppe, I. Gorr, M. Kalocay, H. Richly, and S. Jentsch. 2001. Mobilization of processed, membrane-tethered SPT23 transcription factor by CDC48(UFD1/NPL4), a ubiquitin-selective chaperone. *Cell.* 107:667–677. http://dx.doi.org/10.1016/S0092-8674(01)00595-5

Rebel, A., K. Malkani, M. Basle, C. Bregeon, A. Patezour, and R. Filmon. 1974. Ultrastructural characteristics of osteoclasts in Paget's disease. *Rev. Rhum. Mal. Osteoartic.* 41:767–771.

Roodman, G.D. 2010. Insights into the pathogenesis of Paget's disease. *Ann. N. Y. Acad. Sci.* 1192:176–180. http://dx.doi.org/10.1111/j.1749-6632.2009.05214.x

Roodman, G.D., and J.J. Windle. 2005. Paget disease of bone. *J. Clin. Invest.* 115:200–208. http://dx.doi.org/10.1172/JCI24281

Roodman, G.D., N. Kurihara, Y. Ohsaki, A. Kukita, D. Hosking, A. Demulder, J.F. Smith, and F.R. Singer. 1992. Interleukin 6. A potential autocrine/paracrine factor in Paget's disease of bone. *J. Clin. Invest.* 89:46–52. http://dx.doi.org/10.1172/JCI115584

Rusten, T.E., T. Vaccari, and H. Stenmark. 2012. Shaping development with ESCRTs. *Nat. Cell Biol.* 14:38–45. http://dx.doi.org/10.1038/ncb2381

Ryu, J., H.J. Kim, E.J. Chang, H. Huang, Y. Banno, and H.H. Kim. 2006. Sphingosine 1-phosphate as a regulator of osteoclast differentiation and osteoclast–osteoblast coupling. *EMBO J.* 25:5840–5851. http://dx.doi.org/10.1038/sj.emboj.7601430

Saki, F., Z. Karamizadeh, S. Nasirabadi, S. Mumm, W.H. McAlister, and M.P. Whyte. 2013. Juvenile paget's disease in an Iranian kindred with vitamin D deficiency and novel homozygous TNFRSF11B mutation. *J. Bone Miner. Res.* 28:1501–1508. http://dx.doi.org/10.1002/jbmr.1868

Schweitzer, K., P.M. Bozko, W. Dubiel, and M. Naumann. 2007. CSN controls NF-kappaB by deubiquitinylation of IkappaBalpha. *EMBO J.* 26:1532–1541. http://dx.doi.org/10.1038/sj.emboj.7601600

Shim, J.H., C. Xiao, M.S. Hayden, K.Y. Lee, E.S. Trombetta, M. Pypaert, A. Nara, T. Yoshimori, B. Wilm, H. Erdjument-Bromage, et al. 2006.

CHMP5 is essential for late endosome function and down-regulation of receptor signaling during mouse embryogenesis. *J. Cell Biol.* 172:1045–1056. http://dx.doi.org/10.1083/jcb.200509041

Sims, N.A., and J.H. Gooi. 2008. Bone remodeling: Multiple cellular interactions required for coupling of bone formation and resorption. *Semin. Cell Dev. Biol.* 19:444–451. http://dx.doi.org/10.1016/j.semcdb.2008.07.016

Soriano, P., C. Montgomery, R. Geske, and A. Bradley. 1991. Targeted disruption of the c-src proto-oncogene leads to osteopetrosis in mice. *Cell.* 64:693–702. http://dx.doi.org/10.1016/0092-8674(91)90499-O

Takeshita, S., T. Fumoto, K. Matsuoka, K.A. Park, H. Aburatani, S. Kato, M. Ito, and K. Ikeda. 2013. Osteoclast-secreted CTHRC1 in the coupling of bone resorption to formation. *J. Clin. Invest.* 123:3914–3924. http://dx.doi.org/10.1172/JCI69493

Tang, Y., X. Wu, W. Lei, L. Pang, C. Wan, Z. Shi, L. Zhao, T.R. Nagy, X. Peng, J. Hu, et al. 2009. TGF-beta1-induced migration of bone mesenchymal stem cells couples bone resorption with formation. *Nat. Med.* 15:757–765. http://dx.doi.org/10.1038/nm.1979

Teitelbaum, S.L., and F.P. Ross. 2003. Genetic regulation of osteoclast development and function. *Nat. Rev. Genet.* 4:638–649. http://dx.doi.org/10.1038/nrg1122

Teti, A. 2013. Mechanisms of osteoclast-dependent bone formation. *BoneKEy Rep* 2:449. http://dx.doi.org/10.1038/bonekey.2013.183

Tsang, H.T., J.W. Connell, S.E. Brown, A. Thompson, E. Reid, and C.M. Sanderson. 2006. A systematic analysis of human CHMP protein interactions: additional MIT domain-containing proteins bind to multiple components of the human ESCRT III complex. *Genomics.* 88:333–346. http://dx.doi.org/10.1016/j.ygeno.2006.04.003

van Staa, T.P., P. Selby, H.G. Leufkens, K. Lyles, J.M. Sprafka, and C. Cooper. 2002. Incidence and natural history of Paget's disease of bone in England and Wales. *J. Bone Miner. Res.* 17:465–471. http://dx.doi.org/10.1359/jbmr.2002.17.3.465

Watts, G.D., J. Wymer, M.J. Kovach, S.G. Mehta, S. Mumm, D. Darvish, A. Pestronk, M.P. Whyte, and V.E. Kimonis. 2004. Inclusion body myopathy associated with Paget disease of bone and frontotemporal dementia is caused by mutant valosin-containing protein. *Nat. Genet.* 36:377–381. http://dx.doi.org/10.1038/ng1332

Wei, S., X.M. Dai, and E.R. Stanley. 2006. Transgenic expression of CSF-1 in CSF-1 receptor-expressing cells leads to macrophage activation, osteoporosis, and early death. *J. Leukoc. Biol.* 80:1445–1453. http://dx.doi.org/10.1189/jlb.0506304

Whyte, M.P., C. Tau, W.H. McAlister, X. Zhang, D.V. Novack, V. Preliasco, E. Santini-Araujo, and S. Mumm. 2014. Juvenile Paget's disease with heterozygous duplication within TNFRSF11A encoding RANK. *Bone.* 68:153–161. http://dx.doi.org/10.1016/j.bone.2014.07.019

Xian, L., X. Wu, L. Pang, M. Lou, C.J. Rosen, T. Qiu, J. Crane, F. Frassica, L. Zhang, J.P. Rodriguez, et al. 2012. Matrix IGF-1 maintains bone mass by activation of mTOR in mesenchymal stem cells. *Nat. Med.* 18:1095–1101. http://dx.doi.org/10.1038/nm.2793

Yamanaka, K., Y. Sasagawa, and T. Ogura. 2012. Recent advances in p97/VCP/Cdc48 cellular functions. *Biochim. Biophys. Acta.* 1823:130–137. http://dx.doi.org/10.1016/j.bbamcr.2011.07.001

Zajac, A.J., and P.E. Phillips. 1985. Paget's disease of bone: clinical features and treatment. *Clin. Exp. Rheumatol.* 3:75–88.

Zhao, C., N. Irie, Y. Takada, K. Shimoda, T. Miyamoto, T. Nishiwaki, T. Suda, and K. Matsuo. 2006. Bidirectional ephrinB2-EphB4 signaling controls bone homeostasis. *Cell Metab.* 4:111–121. http://dx.doi.org/10.1016/j.cmet.2006.05.012

Zou, W., H. Kitaura, J. Reeve, F. Long, V.L. Tybulewicz, S.J. Shattil, M.H. Ginsberg, F.P. Ross, and S.L. Teitelbaum. 2007. Syk, c–Src, the alphav-beta3 integrin, and ITAM immunoreceptors, in concert, regulate osteoclastic bone resorption. *J. Cell Biol.* 176:877–888. http://dx.doi.org/10.1083/jcb.200611083